JACS
JOURNAL OF THE AMERICAN CHEMICAL SOCIETY

ARTICLE

pubs.acs.org/JACS

Rh-Catalyzed Polymerization of Phenylacetylene: Theoretical Studies of the Reaction Mechanism, Regioselectivity, and Stereoregularity

Zhuofeng Ke,[†] Satoshi Abe,[‡] Takafumi Ueno,[‡] and Keiji Morokuma*[,†,§]

[†]Fukui Institute for Fundamental Chemistry, Kyoto University, Kyoto 606-8103, Japan

[‡]Institute for Integrated Cell-Material Sciences (iCeMS), Kyoto University, Kyoto 606-8501, Japan

[§]Cherry L. Emerson Center for Scientific Computation and Department of Chemistry, Emory University, Atlanta, Georgia 30322, United States

Supporting Information

ABSTRACT: Poly(phenylacetylene) (PPA) has versatile electrical and optical properties due to its intriguing π-conjugated backbone, configuration, stereoregularity, and helical conformation. Detailed DFT, ONIOM, and ONIOM-MD studies are presented to understand the mechanisms of Rh-catalyzed polymerization of phenylacetylene and the factors that control its regioselectivity and stereochemistry. The polymerization proceeds via the Rh^{I} insertion mechanism ($\Delta H^{\ddagger} \approx 9$ kcal/mol), although all the Rh^{I}, Rh^{III}, and Rh-carbene types of active species are thermodynamically and kinetically plausible in solution; the Rh^{III} insertion and the Rh-carbene metathesis mechanisms both have higher activation enthalpies (~22 and ~25 kcal/mol, respectively). Phenylacetylene prefers a 2,1-inserion, leading to head-to-tail regioselective PPA via a unique π-conjugative transition state. This π-conjugative characteristic specifically favors the 2,1-insertion due to the steric repulsion. Kinetic factors play a key role in the stereoregularity. The polymerization adopting a *cis*−*transoidal* conformation is the most favorable. The kinetic difference for the insertion originates in the conformational constraints of the parent propagation chain in the transition state. These fundamental guidelines should help advance the development of efficient and structurally tailorable PPA catalysts.

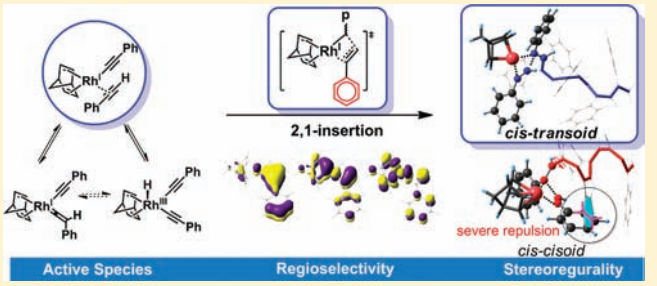

1. INTRODUCTION

The discovery of conducting polymers impacted traditional materials development by combining the electrical and optical properties of metals/semiconductors and the mechanical and processing advantages of polymers.[1,2] With their unique π-conjugated backbones, polyenes offer potential applications in electrical conductivity, photoconductivity, optical nonlinear susceptibility, magnetic susceptibility, liquid crystallinity, etc.[3−7] Poly(phenylacetylene) (PPA), one of the most important materials in the polyenes family, is particularly intriguing due to its solubility in common organic solvents, stability in air, processability, and semiconductor properties.[8,9] In contrast to the unsubstituted polyenes that are symmetric macromolecules, the PPA and its derivatives have versatile chemical and physical properties due to their configuration, stereoregularity, and helical conformation.[7] Today, extensive studies have been invested in the preparation of PPA-type materials, promoted by their high-tech applications as optical polarizing films, asymmetric electrodes, anisotropic molecular devices, chiral sensors and materials with chiral stationary phases, and so on.[6,7,10−15]

Transition-metal-based catalysts for the polymerization of monosubstituted acetylene,[7,16] especially phenylacetylene (PA) (Scheme 1), include group 4 Ti-based catalysts,[17,18] group 6 Mo-/W-based catalysts,[19−21] group 8 Fe-based catalysts,[22−24] group 9 Rh-based catalysts,[25−35] and group 10 Pd-based catalysts.[36−40] Among them, Rh-based catalysts have advantages in efficient living polymerization of PA derivatives in protic solvents, like amines, alcohols, and even environmentally benign water.[25,41−46] Rh-based catalysts are also tolerant toward polar functional groups of PA derivatives.[7,16] Furthermore, Rh-catalyzed PPA has highly *cis*−*transoidal* stereoregularity and can be used to construct screw-sense, helical materials.[6,7]

Scheme 1. Catalyzed Polymerization of Phenylacetylene

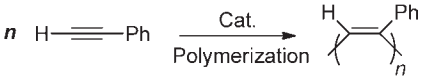

Rh(diene) complexes are typical highly efficient catalysts for the living polymerization of PA, where the bidentate diene ligands are in most cases norbornene (nbd) or 1,5-cyclooctadiene (cod). However, the initiation and propagation mechanisms of the polymerization are complicated and have not yet been completely elucidated.[35,47] As shown in Figure 1(i), an alkynyl-Rh^{I} species could be formed through the deprotonation of a

Received: February 9, 2011
Published: May 02, 2011

dx.doi.org/10.1021/ja2012565 | J. Am. Chem. Soc. 2011, 133, 7926–7941

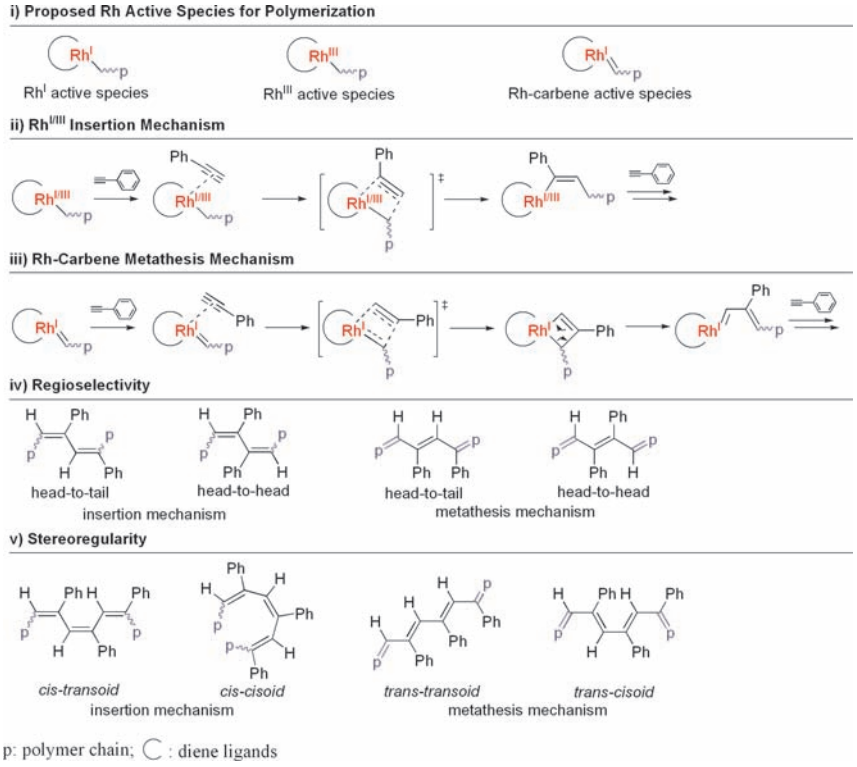

Figure 1. Overview of the mechanistic topics for the Rh-catalyzed polymerization of PA, where p represents a propagation chain.

coordinated PA monomer; however, the formation of a hydride-phenylethynyl-Rh^{III} species via oxidation of the C−H bond of PA or the conversion of PA to a phenylvinylidene ligand, leading to a Rh-carbene species, are also very common in rhodium alkyne chemistry.[48−50] Two general polymerization mechanisms are suggested on the basis of the above plausible species:[31,35] the insertion mechanism via the Rh^{I}/Rh^{III} species and the metathesis mechanism via Rh-carbene species, as shown in Figure 1(ii) and (iii).[51] In the insertion mechanism, the triple bond of PA directly inserts into the Rh−C-p bond, where C-p is the propagation chain. In the metathesis mechanism, the Rh═C double bond performs metathesis with the triple bond of PA, leading to a four-membered-ring intermediate, followed by a ring-opening process to finish the propagation; the triple bond of PA becomes a single bond in the polymer chain. The insertion mechanism was supported by the elegant isotope-labeling studies by Noyori and co-workers.[31] Particularly, the Rh^{I} insertion mechanism was strongly suggested by the isolation of a living intermediate with the polymer chain containing a tetracoordinated Rh^{I} center, whereas the Rh^{III} species was supposed to be involved only in the initiation step. Although Rh^{III} species is generally believed to be inactive for polymerization of alkynes, it was found to be able to catalyze C≡C triple bond insertion.[52−54] Rh^{III} complexes are also reported to promote facile alkene double bond insertion.[55] Rh-vinylidene species have been widely investigated in stoichiometric systems;[48,56−59] Rh-carbene, however, shows different behavior in polymerization of PA as compared to metal-carbenes of earlier transition metals (like Mo or W), which usually predominantly prefer metathesis. Therefore, it is of interest to understand the role of the Rh^{I}, Rh^{III}, and Rh-carbene species during the polymerization of PA and to reveal the relationship between their reactive characteristics and the corresponding reaction mechanisms.

The properties of PPA depend much on its structure. To tailor the PPA structure, it is necessary to understand the exact mechanisms of the polymerization process. As shown in Figure 1-(iv), two PA monomers can be connected head-to-tail or head-to-head, and these are determined by the regioselectivity and the polymerization mechanism. For the insertion mechanism, PA monomers connect with each other by single bonds, while for the metathesis mechanism, PA monomers connect with each other by double bonds. The entire backbone of the PPA that contains alternative single and double bonds can exist in four types of stereoregular structures: the *cis*−*transoidal*, *cis*−*cisoidal*, *trans*−*transoidal*, and *trans*−*cisoidal* structures, as shown in Figure 1(v). PPA produced by Rh catalysts was reported to possess more than 95% *cis* structure, whereas PPA produced by Fe and Mo catalysts contain less *cis* structure; W-based catalysts, in contrast, produce PPA with nearly all *trans* structure.[60] PPA catalyzed by the Ziegler−Natta type of catalysts adopts either a *cis* or *trans* configuration, depending on the temperature; a *cis*-rich polyacetylene observed at low temperature suggested a *cis*-opening mechanism for the Ziegler−Natta type of catalysts.[61] Interestingly, the Rh-catalyzed polymerization of PA usually produces highly pure *cis*−*transoidal* PPA. PPA with high-order chain helicity can also be obtained by altering the substituents of PA, by introducing coordination additives, or by employing external environmental stimuli.[6,7,10−12,62−65] However, until now, it has remained a challenge to selectively produce PPA materials with desired structures, partially because obtaining direct information about the fast propagation step for the polymerization of PA is difficult. From the fundamental mechanistic viewpoint, how is the polymerization selectivity or regularity controlled by the reaction mechanism? Can the regioselectivity or stereoregularity of the PPA be modulated by Rh-based catalysts that have advantages in tolerating polar functional groups and solvents?

dx.doi.org/10.1021/ja2012565 |*J. Am. Chem. Soc.* 2011, 133, 7926–7941

With the above questions in mind, the present theoretical study offers a panoramic view of the polymerization mechanisms and the factors that control its regio-/stereochemistry, with classical diene-rhodium catalyst systems, to provide fundamental understanding and guidelines for the development of efficient and structurally tailorable PPA catalysts.

2. COMPUTATIONAL MODEL AND DETAILS

To fully understand the mechanism, regioselectivity, and stereoregularity for the Rh-catalyzed polymerization of PA, we utilized multiple methods to study the investigated $[Rh(nbd)Cl]_2$ model system, including density functional theory (DFT)[66,67] and the integrated molecular orbital and molecular mechanics method (ONIOM),[68,69] as well as the atom-centered density matrix propagation (ADMP) molecular dynamics modeling at the ONIOM level of theory.[70−72] All the calculations were performed with the GAUSSIAN 09 programs.[73] When studying the initiation process and the propagation mechanism (sections 3.1−3.3), the DFT method with the B3LYP (Becke's three-parameter hybrid functional,[74] LYP correlation functional,[75] and VWN[76]) functional was utilized to fully optimize all the stationary points on the potential energy surfaces (PES) without symmetry or geometric constraints, in conjunction with the Stevens (SBK) triple-ξ valence basis sets and effective core potentials (ECPs) for transition metal rhodium and the 6-31G* basis sets for other elements (termed BS1). It should be noted that different density functionals may vary from each other in predicting reaction barriers. Our evaluation of several typical density functionals showed that they predicted similar results and led to the same discussion and conclusions for the studied rhodium systems (see Table S1 in Supporting Information). Herein we chose the widely used B3LYP method for our study. Frequency calculations at the B3LYP/BS1 level of theory were carried out to confirm stationary points as minima (zero imaginary frequencies) or transition states (one imaginary frequency). The zero-point energies and the thermal correction data were obtained at 298.15 K and 1 atm within the harmonic potential approximation at optimized structures. Intrinsic reaction coordinates (IRCs)[77,78] were performed to verify the connection of the transition states to relevant reactants and products. Single-point calculations were performed to further refine the relative energies with larger basis sets on the basis of the B3LYP/BS1 optimized geometries. The ECP basis sets augmented with additional p and f functions[79,80] were used for rhodium, and 6-311+G** was used for other elements (termed BS2) in these single-point energy calculations. The solvation effect was taken into account by B3LYP/BS2 single-point calculation with integral equation formalism polarizable continuum model (IEFPCM) in water (ε = 78.3553). The radii and nonelectrostatic terms were taken from Truhlar and co-workers' universal solvation model (SMD).[81] In sections 3.3 and 3.4, to give deeper insight into the regioselectivity and stereoregularity during the polymerization, the two-layer ONIOM calculations were employed with more realistic models possessing a model propagation chain, where the important reaction region was treated quantum mechanically with the DFT method, while the contribution of interactions from the rest of the model was treated with the universal force field (UFF),[82] in which the interface between the QM and MM regions was treated by hydrogen link atoms. The ONIOM optimization, frequency and IRC calculations were performed at the B3LYP/BS1:UFF level of theory in the gas phase. ADMP simulations were also carried out with a two-layer ONIOM scheme in the gas phase (298.15 K and 1 atm). For computational facility, the QM part was treated with the B3LYP/LANL2MB level of theory during the MD simulation. The step size in dynamics is set to be 0.2 fs. Similar to the DFT calculation described above, the higher level single-point calculation and IEFPCM calculation with SMD solvation model (oniompcm=x) were also carried out at the (B3LYP/BS2:UFF)//(B3LYP/BS1:UFF) level of theory to obtain the solvent-corrected ONIOM enthalpies and free energies. All the solvent-corrected enthalpies and free energies for the studied stationary points are listed in the paper and the Supporting Information. Both enthalpy and free energy data lead to the same discussion and conclusions for our studied systems. Considering the contribution of translational and rotational entropy might lead to increased errors for solvent-corrected free energies; thus, the discussion throughout the text is based on the solvent-corrected enthalpies.

Scheme 2. Interchanges among the Phenylethynyl-Rh^{I}, Hydride-phenylethynyl-Rh^{III}, and Phenylvinylidene-Rh^{I} Species in Solution[a]

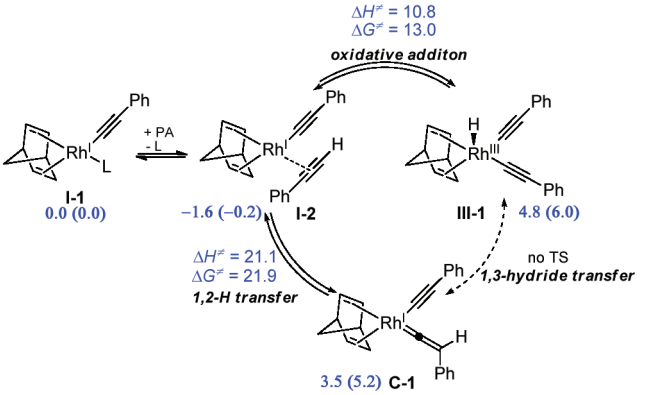

[a] Solvent-corrected enthalpies and free energies (in parentheses) are in kcal/mol, relative to **I-1**; only the energies of the most feasible pathway for each step are listed here; detailed information about the equilibria is summarized in the Supporting Information.

3. RESULTS AND DISCUSSION

3.1. Plausible Active Species. The classical $[Rh(nbd)Cl]_2$ system was chosen as the model catalyst to study the polymerization of PA. As shown in Scheme 2, we took the alkynyl-Rh^{I} species **I-1** as the starting point, where L is the solvent molecule water. Experimental observation demonstrated that the deprotonation of a η^2-alkyne ligand from catalyst precursors produced an alkynyl-Rh complex for the subsequent polymerization.[35,83] In experiments, bases, like sodium hydroxide, sodium tetraphenylborate, silver triflate, and amines, are generally used to abstract the chloride ligand of the catalyst precursor or the acidic hydrogen of PA in the initiation stage.[7,64,84] The living polymerization of PA can also be achieved by directly using alkynyl as a ligand in the precursors.[31,35,85,86] However, without additive base, only $[Rh(diene)Cl]_2$ did not promote the polymerization of PA in toluene.[87]

The starting phenylethynyl-Rh(I) species **I-1** can easily coordinate with a PA monomer, accompanied with the release of solvent molecule. Transformations among alkyne, alkynyl, and vinylidene are very common in transition metal systems.[48] Therefore, plausible active species for the Rh-catalyzed polymerization of PA could, theoretically, include alkynyl-Rh^{I}, hydride-alkynyl-Rh^{III}, or vinylidene-Rh^{I} species. Although these kinds of structures were reported to be captured or even characterized by X-ray diffraction in other stoichiometric systems,[56−59,88−92] the direct observation of hydride-Rh^{III} and vinylidene-Rh^{I} is rather challenging,[31,35] probably due to the complicated and fast polymerization process. We first evaluated the thermodynamic

dx.doi.org/10.1021/ja2012565 |J. Am. Chem. Soc. 2011, 133, 7926–7941

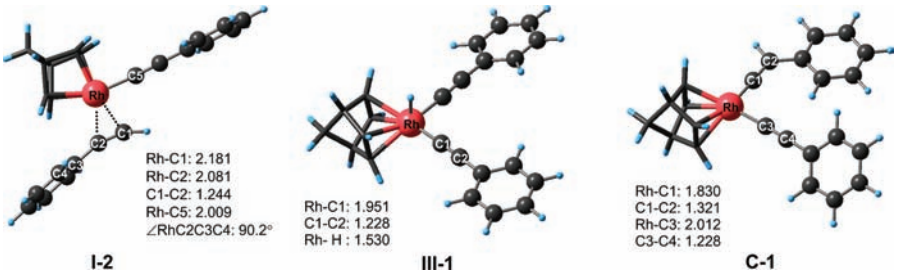

Figure 2. Optimized structures of **I-2**, **III-1**, and **C-1** species. Bond lengths are in angstroms.

and kinetic possibility of the existence of these plausible active species in the reaction system, as shown in Scheme 2. Our results indicate that the interchanges among the phenylethynyl-Rh^{I} (**I-2**), hydride-phenylethynyl-Rh^{III} (**III-1**), and phenylvinylidene-Rh^{I} (**C-1**) species are all thermodynamically and kinetically feasible at room temperature in solution.

*Phenylethynyl-Rh^{I} Species (**RhI**), **I-1***. The formation of the metal-alkyne intermediate **I-2** from **I-1** by replacement of the solvent molecule with monomer PA is slightly downhill by 1.6 kcal/mol in solution. The optimized structure of **I-2**, shown in Figure 2, is consistent with other typical experimental and computational structures,[49,93,94] with bond lengths Rh−C^1 = 2.181 Å, Rh−C^2 = 2.081 Å, and C^1−C^2 = 1.244 Å. Actually, **I-2** has two other isomers. One has a coordinated triple bond perpendicular to the square-planar surface of the complex, and the other has a parallel-coordinated PA like **I-2**, with the phenyl of PA *cis* to the phenylethynyl ligand. No isomer with a M···C−H agostic interaction was obtained as a minimum. These three isomers of **I-2** have quite similar stabilities. The enthalpy differences among them are smaller than 2.1 kcal/mol, and **I-2** is the most stable one (Scheme 1S, Supporting Information). We similarly carefully checked all the possible isomers for each species of our study and discuss the most stable ones through the text.

*Hydride-phenylethynyl-Rh^{III} Species (**RhIII**), **III-1***. Oxidative addition of the acidic C−H bond of the coordinated PA leads to the hydride-phenylethynyl-Rh^{III} intermediates, **III-1**. We found that the formation of **III-1** is uphill by 4.8 kcal/mol relative to the starting point, **I-1**. The transition-state enthalpy for this oxidative addition is only 10.8 kcal/mol relative to **I-1**, indicating that there is a facile equilibrium between **I-2** and **III-1** in solution at room temperature. This oxidative addition can proceed through a dissociative mechanism or an associative mechanism. Further details are given in the Supporting Information (Scheme S2, Figure S1). Actually, the oxidative addition of alkyne is a widely studied process in rhodium alkyne chemistry.[48] Some examples of the structures of related hydride-alkynyl-Rh^{III} intermediates can be seen in the literature.[89−91] Our optimized structure (Figure 2) of **III-1** has bond lengths Rh−C^1 = 1.951 Å, C^1−C^2 = 1.228 Å, and Rh−H = 1.530 Å. For comparison, the ranges of the bond lengths of Rh−C, C≡C, and Rh−H in experimental examples are 1.95−1.97, 1.21−1.22, and 1.44−1.66 Å, respectively.[89−91] The optimized structure of **III-1** reproduces well the typical hydride-alkynyl-Rh^{III} structures reported in the literature.

*Carbene-Type Phenylvinylidene-Rh^{I} Species (**RhC**), **C-1***. Conversion between alkyne and vinylidene has been widely investigated by experimentalists[48,56−59] and theoretical chemists for different systems.[49,50,95−97] It is generally suggested that this process may occur via two mechanisms. One is direct 1,2-hydrogen transfer, and the other is oxidative addition followed by a 1,3-hydride transfer through a hydride-Rh^{III} intermediate. Although a bimolecular reaction was also suggested for the hydride-transfer step, labeling experiments strongly supported a unimolecular process.[97−100] Our study found (Scheme 2) that 1,2-H transfer from the coordinated PA directly leads to the formation of phenylvinylidene-Rh^{I} species, **C-1**, with the reaction barrier of 22.7 kcal/mol in solution relative to **I-2**, which is quite similar to other experimental and computational results. Careful verification along the IRC path proved that the 1,2-H transfer transition state indeed connects with **I-2** and **C-1**. It should be noted that no transition state was obtained for the 1,3-hydride transfer from **III-1** to **C-1** after extensive attempts. A relaxed scan found that the 1,3-hydride transfer is actually a stepwise process including both oxidative addition of the C−H bond and 1,2-hydrogen transfer. As compared with the formation of **I-1** and **III-1**, the formation of carbene-type **C-1** is less feasible. The enthalpy of **C-1** is uphill by 3.5 kcal/mol, and the reaction barrier from **I-2** to **C-1** is relative high. However, we will keep this carbene intermediate as a plausible active species for the polymerization of PA, since the reaction barrier of 22.7 kcal/mol may still be feasible for the reaction at room temperature. These d^8 Rh^{I} and d^6 Rh^{III} complexes usually exist in singlet ground states. As expected, the triplets **I-1**, **C-1**, and **III-1** are calculated to be higher in enthalpies than their singlet states by 27.5, 24.8, and 44.0 kcal/mol, respectively. These high spin state species should be excluded as active species for the polymerization of PA.

*Electronic and Reactive Characteristics of the **RhI**, **RhIII**, and **RhC** Types of Active Sites.* Having shown that all the **RhI**, **RhIII**, and **RhC** types of active species may be thermodynamically and kinetically feasible at room temperature in solution, we need to further understand the different electronic characteristics and reactivity of these active sites and how these properties would affect their polymerization activities.

As shown in Figure 3, the **RhI** species must release a ligand to generate a **RhI** active species for the polymerization. This **RhI** active site has a d^8 electronic configuration. Except for the other four filled d orbitals, the empty $d_{x^2-y^2}$, which mixes with the metal p orbital, serves as an electrophile for the approaching PA monomer. The HOMO is a π^* orbital located mainly at the alkynyl ligand (or alkenyl during the propagation) and serves as a nucleophile, having an increased nucleophilic ability due to the perturbation by metal d orbitals. The cooperative electrophilic attack of d_{x^2-y} onto the π orbital of PA and nucleophilic attack of the HOMO orbital to the π^* orbital of PA lead to insertion at the PA triple bond.

The **RhIII** active species has reactivity characteristics similar to **RhI**, except that the Rh^{III} is a high oxidation state possessing a d^6 electronic configuration in which the empty d_{z^2} serves as an electrophile. Due to the high oxidation state, the **RhIII** d_{z^2} orbital is a better electrophile than the **RhI** d_{x^2-y} orbital. However, the

dx.doi.org/10.1021/ja2012565 |*J. Am. Chem. Soc.* 2011, 133, 7926–7941

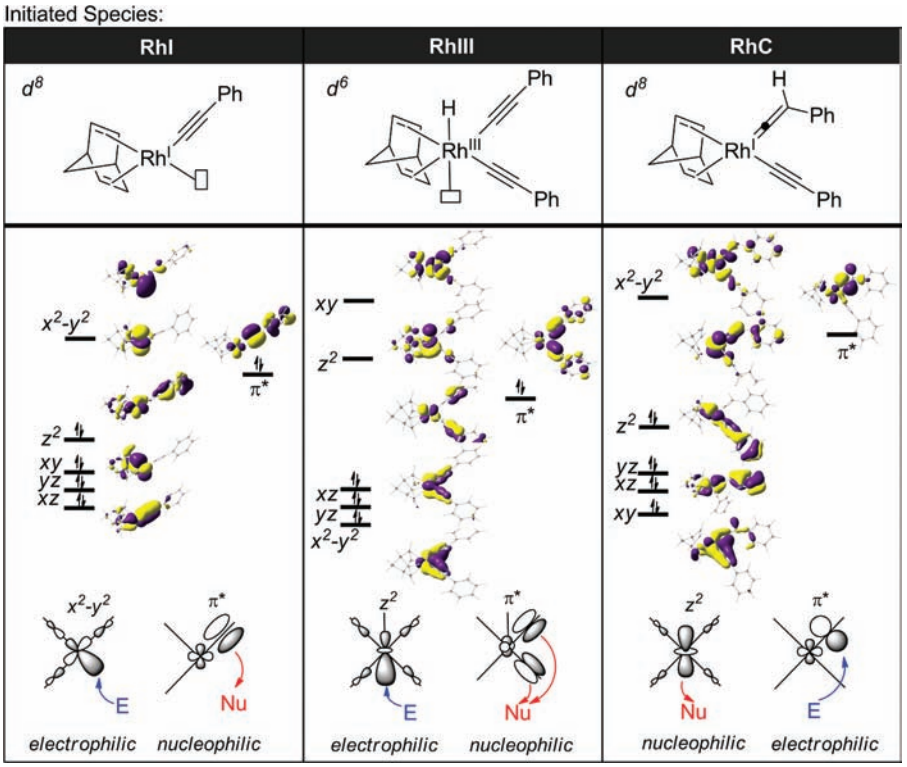

Figure 3. Electronic configuration and reactivity characteristics of **RhI**, **RhIII**, and **RhC** species.

HOMO in **RhIII** becomes less nucleophilic than the HOMO in **RhI**, due to reduced perturbation by the metal d orbital. Furthermore, during the coordination of the PA monomer, d back-donation plays an important role. The Rh^{I} metal center has a better back-donating ability than Rh^{III} does. All these factors should have considerable effects on the polymerization activities for the **RhI** and **RhIII** active species.

The **RhC** active species is a Fischer-type carbene, with an electrophilic π^* orbital on the vinylidene ligand. **RhC** has a metal center with low oxidation state, in which the electronic configuration is d^8. As shown in Figure 3, except for the $d_{x^2-y^2}$ orbital, all four other d orbitals are already filled. Thus, the highest filled d orbital, d_{z^2}, serves as a nucleophile to attack the π^* orbital of PA during the metathesis; meanwhile, the electrophilic π^* orbital on the vinylidene ligand accepts the π electrons from PA, indicating a totally different reactivity characteristic compared to **RhI** and **RhIII**.

3.2. Initiation and Polymerization Mechanisms. With the different electronic characteristics of the **RhI**, **RhIII**, and **RhC** types of active species in mind, we further investigated the different polymerization behaviors promoted by them, i.e., the Rh^{I} insertion, Rh^{III} insertion, and Rh-carbene metathesis pathways. Besides the fundamental chemistry of the behavior of the polymerization mechanism, we also discuss the initial insertion process during the polymerization. The discussed reaction pathways are shown in Scheme 3. The PES results are depicted in Figure 4. Key intermediate and transition-state structures are shown in Figure 5. It should be noted that our discussion focuses on the most favorable pathway for each investigated mechanism. Besides the most favorable pathway, we also extensively investigated other theoretically possible reaction pathways for each mechanism. Their PESs and corresponding transition-state isomers are summarized in the Supporting Information (Figure S2−S5 for Rh^{III} insertion; Scheme S5, Figures S6 and S7 for Rh-carbene metathesis).

Rh^{I} Insertion Mechanism. Rh^{I} insertion starts from the replacement of the solvent molecule with the monomer PA to form **I-2**. In **I-2**, back-donation of the Rh d electrons activates the C≡C triple bond of the coordinated PA (bond length, 1.244 Å, Figure 2) from that of the free PA (1.210 Å). The activated PA can more easily undergo an insertion to the phenylethynyl ligand via a four-membered ring transition state, **I-TS1**. In **I-TS1**, the π electrons of the triple bond are donated to the metal center to form an $Rh-C^2$ bond (2.081 Å), while the phenylethynyl ligand leaves the metal center to interact with the C^1 atom (C^1-C^5 = 1.935 Å) and the triple bond breaks further (1.287 Å). Insertion via **I-TS1** has a reaction barrier of 13.3 kcal/mol relative to **I-2**. Formation of the insertion product **I-3** is exothermic by 15.3 kcal/mol with respect to **I-1**. The second insertion process also starts with the coordination of monomer PA. The coordination enthalpy of PA (from **I-3** to **I-4**) is −9.3 kcal/mol. From **I-4**, the insertion step of the second PA is even easier ($\Delta H^{\ddagger}$ = 9.4 kcal/mol) than the first one discussed above. **I-TS1/2** has other transition-state isomers related to other pathways, which produce different regioselective or stereoselective products. The origin of regioselectivity and stereoregularity will be discussed in sections below. The transition state **I-TS1/2** has the lowest energy compared to other insertion transition-state isomers. Note that **I-TS1**, where the C≡C bond inserts to an sp-hybridized carbon, represents the TS for the first insertion, while **I-TS2** represents an insertion of the C≡C bond to an sp^2-hybridized carbon and is the representative TS for the propagation steps. The insertion to the sp^2-hybridized carbon is more facile due to lower constraint in the four-membered ring transition

dx.doi.org/10.1021/ja2012565 |*J. Am. Chem. Soc.* 2011, 133, 7926–7941

Scheme 3. Mechanisms for the Rh-Catalyzed Polymerization of PA (pel = phenylethynyl)

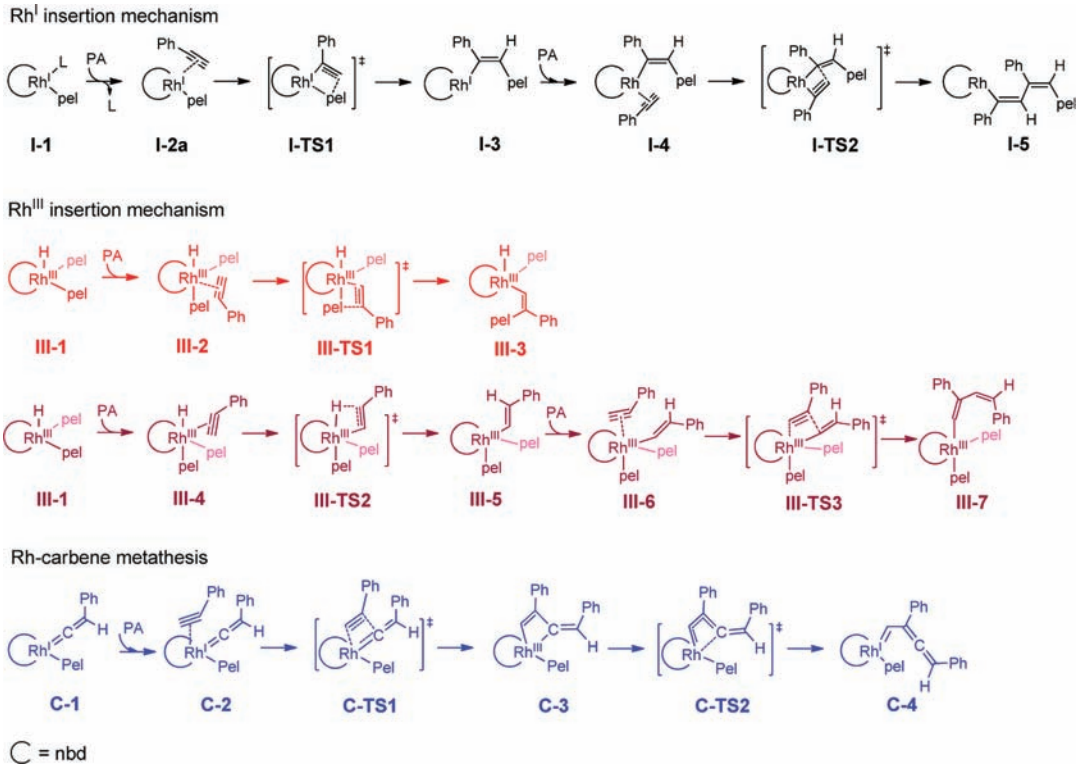

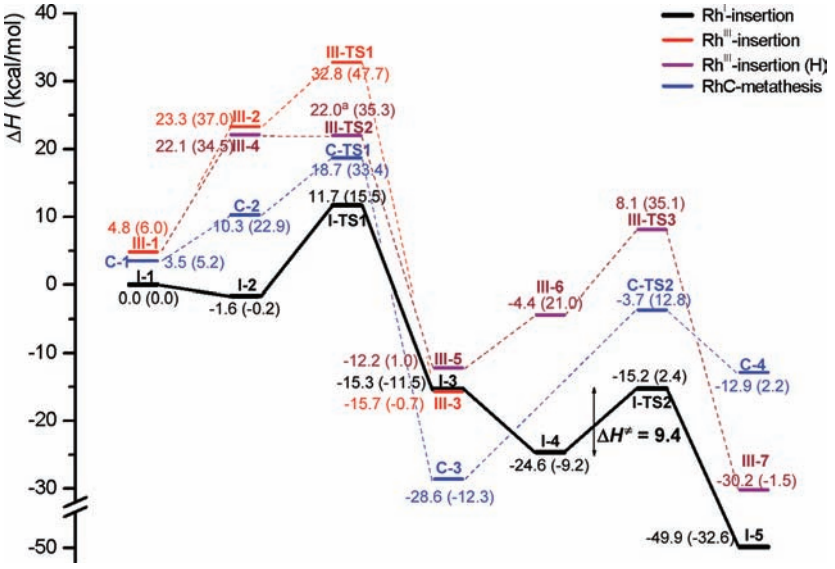

Figure 4. PES profiles for the reaction mechanisms of the Rh-catalyzed polymerization of PA. Solvent-corrected enthalpies and free energies (in parentheses) are in kcal/mol, relative to starting point **I-1**. Only the most favorable pathway for each mechanism is shown; detailed information about other reaction pathways is given in the Supporting Information. [a]The enthalpy of **III-TS2** is higher than that of **III-4** by 1.8 kcal/mol without solvation correction.

structure. It is expected that the insertion of the third and subsequent PA monomers during the propagation stage takes place via a TS which is similar in structure and energy to **I-TS2**. Our calculation indicates an average reaction barrier for the propagation process of Rh^{I} insertion mechanism to be ~9.4 kcal/mol.

Rh^{III} Insertion Mechanism. The Rh^{III} insertion is found to proceed in a similar fashion to Rh^{I} insertion but is energetically much less feasible. From **III-1**, the Rh^{III} insertion can proceed via two different pathways (Scheme 3 and Figure 4): one is the insertion of PA into the Rh−pel bond (C−C coupling); the other is the insertion of PA into the Rh−H bond (C−H coupling). The coordination of PA to form complex **III-2** or **III-4** is highly uphill by 23.3 or 22.1 kcal/mol, respectively. The highly energetically unfavorable coordination of PA can be

dx.doi.org/10.1021/ja2012565 |*J. Am. Chem. Soc.* 2011, 133, 7926–7941

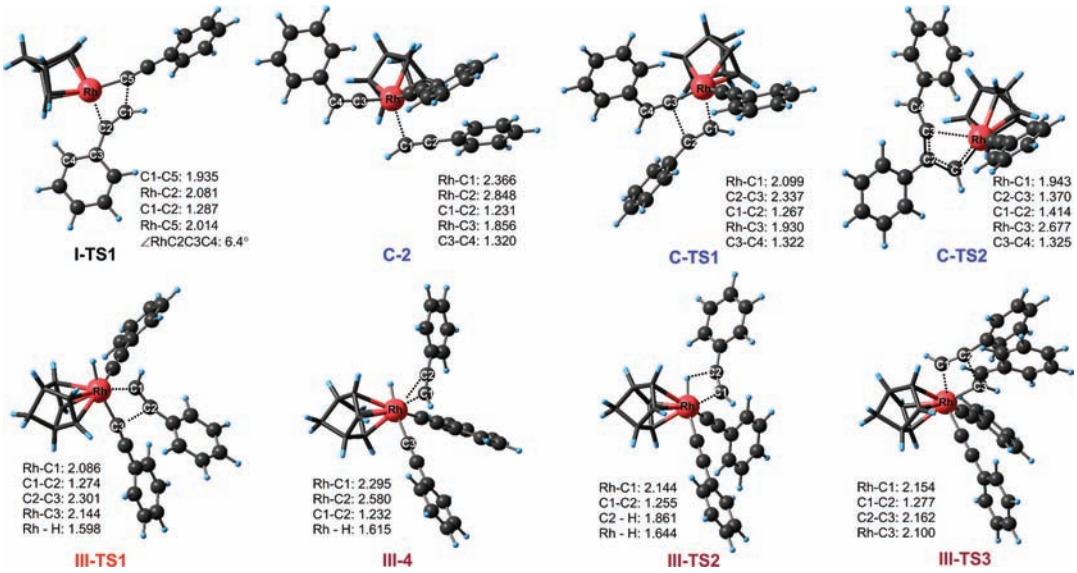

Figure 5. Optimized structures of the key intermediates and transition states for the Rh^{I} insertion, Rh^{III} insertion, and Rh-carbene metathesis mechanisms. Bond lengths are in angstroms.

attributed mainly to the solvation effect. In solution, the vacant site is expected to be stabilized strongly by solvent. Compared to Rh^{I}, Rh^{III} is a harder metal center and more prefers the water solvent than the monomer PA. Overall, the Rh^{III} insertion step is required to overcome a barrier of 32.8 kcal/mol (**III-TS1**) for the C−C coupling pathway and a barrier of 22.0 kcal/mol (**III-TS2**) for the C−H coupling pathway. In the C−H coupling pathway, the second step is the insertion of C≡C bond inserts into an sp^2-hybridized carbon (**III-5** → **III-7**) and represents the propagation steps for the Rh^{III} insertion mechanism. The reaction barrier of **III-TS3** with respect to **III-5** is calculated to be 20.3 kcal/mol. Therefore, it can be expected that the Rh^{III} insertion mechanism has a propagation barrier of ∼20 kcal/mol, which is higher than that of the Rh^{I} insertion ($\Delta H^{\ddagger}$ = 9.4 kcal/mol). Considering the structural and electronic characteristics of Rh^{III} species, Rh^{III} is not a good active species for the PA insertion for the following reasons: (i) The Rh^{III} center has a poor binding capability toward the triple bond of PA, because of the weak d−π donation as well as the sterically hindered environment. The weak coordination interaction is obvious in, for example, the structure of **III-4**, where the Rh−C^2 distance is 2.580 Å (Figure 4), much shorter than that of **I-2** (2.081 Å, Figure 2). The C≡C triple bond length of PA (1.232 Å) in **III-4** is also shorter than that of **I-2** (1.244 Å). (ii) The nucleophilicity of the π^* orbital (HOMO) of the Rh^{III} species is relatively weak, because the high oxidation state of the metal center decreases the d−π mixing. The nucleophilic π^* orbital of **RhIII** (Figure 3) is calculated to have an energy of −0.19317 au, while the energy of the nucleophilic π^* orbital of **RhI** is −0.18969 au.

Rh-Carbene Metathesis Mechanism. The Rh-carbene species can undergo a metathesis transformation with the triple bond of PA, followed by a ring-opening of the four-membered ring carbometalate intermediate. Because the Rh-carbene species has a filled d_{z^2} orbital, there is no direct interaction between the d_{z^2} orbital and π electrons of the C≡C triple bond. Generally speaking, the nucleophilic d_{z^2} orbital may interact weakly with the π^* orbital of the C≡C triple bond. However, we could not locate this kind of intermediate. The acidic C−H bond of PA is more easily attracted by π electrons of the alkynyl ligand in the gas phase. The coordination of PA to **C-1** forces **C-2** to adopt a quasi-pyramidal structure. The Rh−C^1 bond length is 2.366 Å. **C-2** is higher in enthalpy than **C-1** by 6.8 kcal/mol and higher than **I-1** by 10.3 kcal/mol. The activation enthalpy of metathesis transition state **C-TS1** is 18.7 kcal/mol. However, the subsequent ring-opening step via **C-TS2** has to overcome a reaction barrier of 24.9 kcal/mol, relative to intermediate **C-3**. Remember that the formation of Rh-carbene species (**I-2** → **C-1**) also needs to overcome a barrier of 22.7 kcal/mol. Compared with the low activation enthalpy of Rh^{I} insertion (13.3 kcal/mol for the first insertion, 9.4 kcal/mol for subsequent insertion for propagation), the Rh-carbene metathesis mechanism is suggested to be less feasible for the polymerization of PA. More importantly, the four-membered ring carbometalate intermediate **C-3** is predicted to be relatively too stable, making the subsequent ring-opening an endothermic process (**C-3** → **C-4**, ΔH = 15.7 kcal/mol). Therefore, incorporation of the PA monomer into the propagation chain via metathesis is thermodynamic prohibited. Actually, without competition from triple bond insertion, the rhodium four-membered ring carbometalate intermediate could be trapped in proper stoichiometric experiments.[101−103] It could be expected that decreasing the stability of the carbometalate intermediate may make the whole metathesis and ring-opening process thermodynamically possible. For example, using a harder transition metal is helpful to decrease its interaction with soft carbon. Our results showed that Rh catalyst prefers an insertion polymerization of PA rather than metathesis polymerization via Fischer-type metal-carbene species. When the metal-carbene resembles more a Schock-type, the polymerization may have a different mechanistic story due to the change in the reactivity characteristics.

Our calculated results thus strongly supported the Rh^{I} insertion mechanism to be the most feasible mechanism for the polymerization ($\Delta H^{\ddagger}$ = 9.4 kcal/mol), which is well consistent with Noyori and co-worker's ^{13}C-labeling experiments resulting in a double $^{13}C{=}{=}^{13}C$ bond character.[31] The Rh^{III} insertion mechanism is less possible, with a propagation barrier of 20.3 kcal/mol. With respect to the Rh-carbene metathesis process, it is even more

dx.doi.org/10.1021/ja2012565 |*J. Am. Chem. Soc.* 2011, 133, 7926–7941

Scheme 4. Reaction Pathways To Prevent the Incorporation of Isotope-Labeled $-^{13}C\equiv{}^{13}CPh$ Ligand into the Polymer Chain[a]

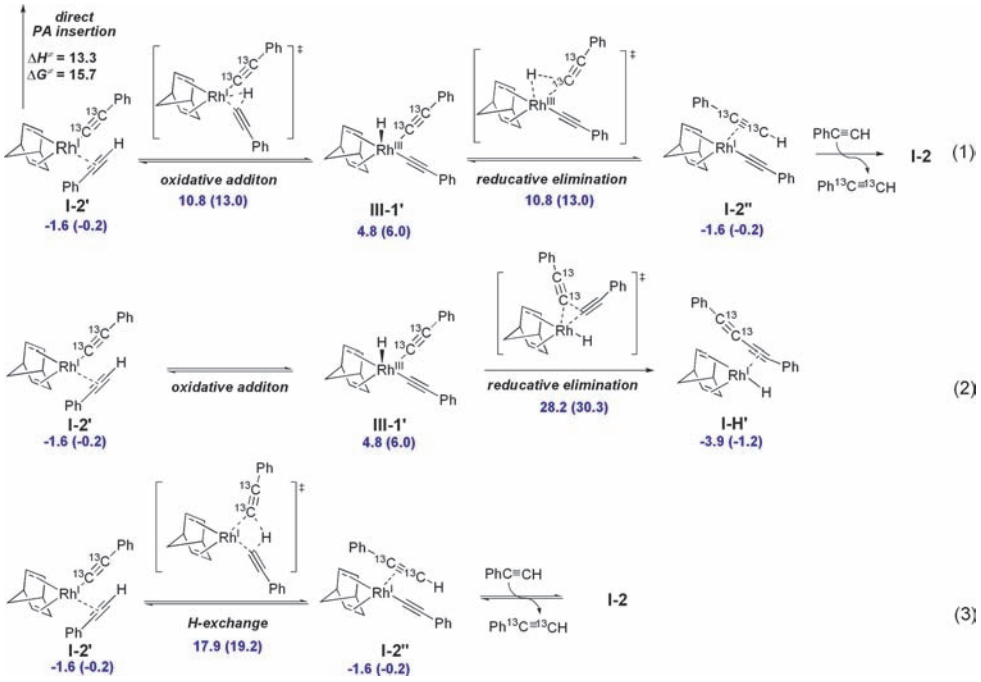

[a] Solvent-corrected enthalpies and free energies (in parentheses) are in kcal/mol, relative to **I-1**; detailed information about the equilibria is summarized in the Supporting Information.

difficult due to (i) its highly endothermic ring-opening step and (ii) its rate-determining step, which has a reaction barrier of 24.9 kcal/mol.

Initial Insertion Process. It was previously suggested that monomer PA did not directly insert into the Rh-phenylalkynyl bond in the initiation step. Experimental studies found that an isotope-labeled $-^{13}C\equiv{}^{13}CPh$ ligand in the catalyst precursor was not detected to be incorporated into the polymer products.[31] A possible explanation was that the oxidative addition of PA leads to a subsequent reductive elimination of $PhC\equiv C-{}^{13}C\equiv{}^{13}CPh$, which may result in a rhodium hydride species as an initiator for the polymerization.[31,104] Recent experiments also suggested an alkynyl ligand could have an active role in the initiation process,[35,85] and no Rh-hydride species or $PhC\equiv C-C\equiv CPh$ was observed in the reaction mixture.[35] Our DFT study provides interesting insights with the catalyst model to further understand the initiation process.

Upon adding monomer PA to the catalyst precursor with an isotope-labeled $-^{13}C\equiv{}^{13}CPh$ ligand, there are three possible ways to release the $-^{13}C\equiv{}^{13}CPh$ ligand.[31,35,105] We found that there exists a quick equilibrium between phenylethynyl-Rh^{I} intermediate **I-2′** and hydride-diphenylethynyl-Rh^{III} **III-1′**, as shown in eq (1) of Scheme 4. Actually, oxidation of the C−H bond of PA has a barrier of only 12.4 kcal/mol relative to **I-2′**. In this equilibrium, the isotope-labeled $-^{13}C\equiv{}^{13}CPh$ ligand can be released to the solution via the process shown in eq (1). The released $H^{13}C\equiv{}^{13}CPh$ has much lower concentration in the solution than PA monomer. Once released in solution, the low concentration of $H^{13}C\equiv{}^{13}CPh$ makes it unlikely to re-incorporate into the complex. Additionally, $H^{13}C\equiv{}^{13}CPh$ has lower reactivity in C−H oxidation addition than PA due to the isotope effect. This quick pre-equilibrium can well explain why isotope-labeled alkynyl group was not incorporated into the polymer.

In contrast, elimination of $PhC\equiv C-{}^{13}C\equiv{}^{13}CPh$ to form hydride-Rh^{I} species **I-H** is found to be less feasible during the initial insertion process. As shown in eq (2) of Scheme 4, the C−C reductive elimination is calculated to have an activation enthalpy of 28.2 kcal/mol, which is much higher than that of the C−H reductive elimination and also higher than that of the direct insertion for the polymerization (13.3 kcal/mol). The transformation from **III-1** to **I-H** is complicated, with several possible reaction pathways; detailed transformation about associated/dissociated mechanisms is given in the Supporting Information (Schemes S3 and S4, Figure S1). It can be expected that only in a stoichiometric system, where the ratio of catalyst precursor to the monomer is high, could the formation of $PhC\equiv C-C\equiv CPh$ be detected as a side reaction.[35] The elimination of the isotope-labeled $-^{13}C\equiv{}^{13}CPh$ ligand may also proceed via hydrogen exchange between monomer and the phenylethynyl ligand, as shown in eq (3) of Scheme 4. This process, with a barrier of 19.5 kcal/mol, is easier than the reductive elimination of $PhC\equiv C-C\equiv CPh$ but more difficult than the C−H oxidative addition/reductive elimination equilibrium.

3.3. Regioselectivity. With the new understanding of the polymerization mechanism, we further investigate the regioselectivity of PA insertion. In the Rh^{I} insertion mechanism, the PA may have different regioselectivities, i.e., 1,2-insertion and 2,1-insertion (Chart 1), leading to either head-to-head or head-to-tail connection (Figure 1) depending on the regioselectivity of the previous insertion. Using isotope-labeled PA as monomer, Noyori and co-workers elegantly demonstrated the 2,1-regioselectivity during polymerization, which led to a head-to-tail backbone structure.[31] To reveal the origin of the regioselectivity, as well as to provide helpful guideline for the development of regioselectivity-controllable catalysts, we further compared the regioselectivity between 1,2-insertion (in green) and 2,1-insertion

dx.doi.org/10.1021/ja2012565 |J. Am. Chem. Soc. 2011, 133, 7926–7941

(in black) for the Rh-catalyzed polymerization of PA. The obtained PESs are summarized in Figure 6. The 2,1-insertion of PA into the phenylethynyl-Rh bond via transition state **I-TS1** has a reaction barrier of 13.3 kcal/mol, which is lower than that of the corresponding 1,2-insertion (via **I-TS1a**) by 3.5 kcal/mol. Both the 2,1- and 1,2-insertion steps are highly exothermic. The formed 1,2-insertion product **I-3a** has stability similar to that of the 2,1-insertion product **I-3**. Starting with **I-3**, the second insertion can also occur via either 1,2- or 2,1-insertion of PA into an alkenyl-Rh bond. Similarly, the coordination of PA to **I-3** leads to two complex isomers, **I-4** and **I-4a**. **I-4** corresponds to 2,1-insertion through transition state **I-TS2**, while **I-4a** leads to 1,2-insertion via transition state **I-TS2a**. Again, the 2,1-insertion transition state **I-TS2** is lower in enthalpy than the 1,2-insertion transition state **I-TS2a**, with larger regioselectivity of $\Delta\Delta H^{\ddagger}$ = 5.4 kcal/mol.

We initially suspected that both steric and electronic effects of the phenyl group in PA may play important roles in the regioselectivity. Although the linear phenylethynyl ligand is not a bulky group, the selectivity between **I-TS1** and **I-TS1a** is still considerable ($\Delta\Delta H^{\ddagger}$ = 3.5 kcal/mol). Interestingly, when a simple model with a small hydride as ligand (instead of phenylethynyl, see Figure 7) was used to test the electronic effect on the regioselectivity, we found that the insertion of PA shows no preference for either 1,2- or 2,1-insertion. The enthalpies of **I-TS3** and **I-TS3a** are exactly the same in the gas phase; with solvation effect correction, **I-TS3** is slightly favored over **I-TS3a** by only 0.1 kcal/mol. There is no regioselectivity for this model with hydride ligand.

Chart 1. 2,1-Insertion and 1,2-Insertion

Carefully checking the structures of **I-TS3** and **I-TS3a**, we found a unique conjugative characteristic in the insertion transition state, which requires the phenyl group to locate on the square-planar surface of the rhodium complex. In PA, there are two sets of π orbitals for the C≡C triple bond; one is parallel to the π orbitals of the phenyl group and is named $\pi_{\|}$, as shown in the right of Figure 8(i), while the other one ($\pi_{\perp}$) is perpendicular to the phenyl π orbitals. As illustrated in section 3.1, during Rh^{I} insertion process, one set of PA π and π^* orbital acts as nucleophile and electrophile to react with the d_{x^2-y} and π^* orbitals of **RhI**, respectively, as shown in Figure 8(ii). Generally speaking, the $\pi_{\|}/\pi_{\|}^*$ should be more nucleophilic/electrophilic due to the conjugated perturbation of the phenyl group. However, our study found a transition state for the insertion with significant π-conjugative characteristic, where the PA $\pi_{\perp}/\pi_{\perp}^*$ are actually involved in the σ bond formation with Rh center. As shown in the left of Figure 8(ii), the d orbital of the rhodium center participates in a significant conjugated interaction with monomer PA during the insertion. In contrast, a perpendicular transition state breaks the conjugative system of PA, as shown in the right of Figure 8(ii). This is further evidenced by the $\angle RhCCC^{phenyl}$ dihedral angle in both **I-TS3** and **I-TS3a**: they are nearly perfectly 0°, indicating that the phenyl group is coplanar with the PA C≡C triple bond and the Rh atom. The Rh d_{π} orbital, the nbd π acceptors, and the π system of PA tend to form a conjugative network with the conjugative system of PA to gain extra stabilization energy during the insertion, as illustrated in the MO diagram of Figure 8(iii).

In the conjugative insertion TS, the small hydride ligand does not cause steric repulsion for both 1,2-insertion and 2,1-insertion, resulting in no preference between them. However, the replacement of hydride in **I-TS3a** with a phenylethenyl group to give **I-TS2a** will cause significant steric repulsion for the C^4—H fragment of PA. As a consequence, we can see that the 2,1-insertion is preferred by 3.5 and 5.4 kcal/mol for phenylethynyl and phenylethenyl ligands, respectively. To evaluate the average

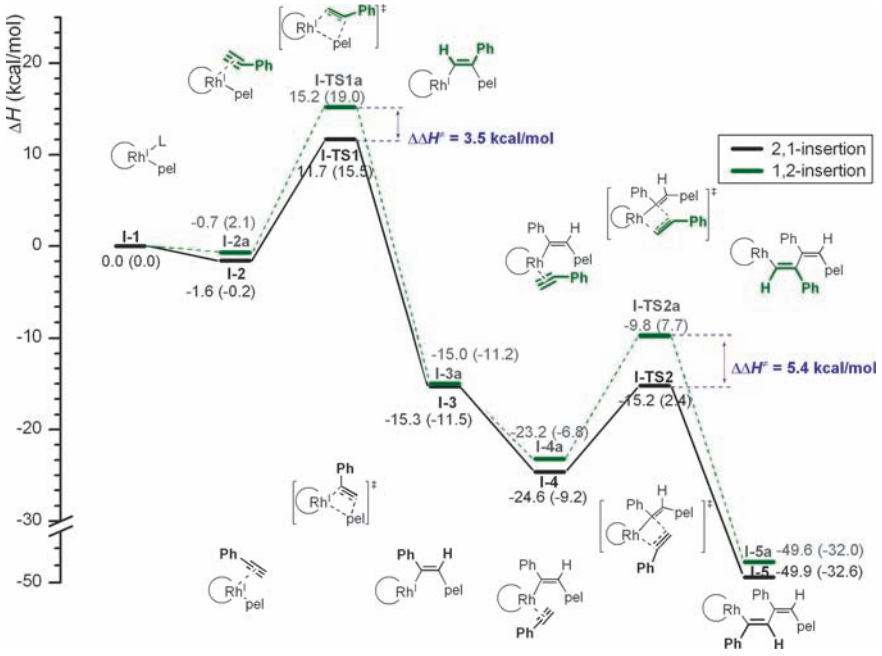

Figure 6. PES profiles for the regioselectivity of PA insertion (pel = phenylethynyl; nbd ligand is simplified as a curve for clarity). Solvent-corrected enthalpies and free energies (in parentheses) are in kcal/mol, relative to starting point **I-1**.

dx.doi.org/10.1021/ja2012565 |*J. Am. Chem. Soc.* 2011, 133, 7926–7941

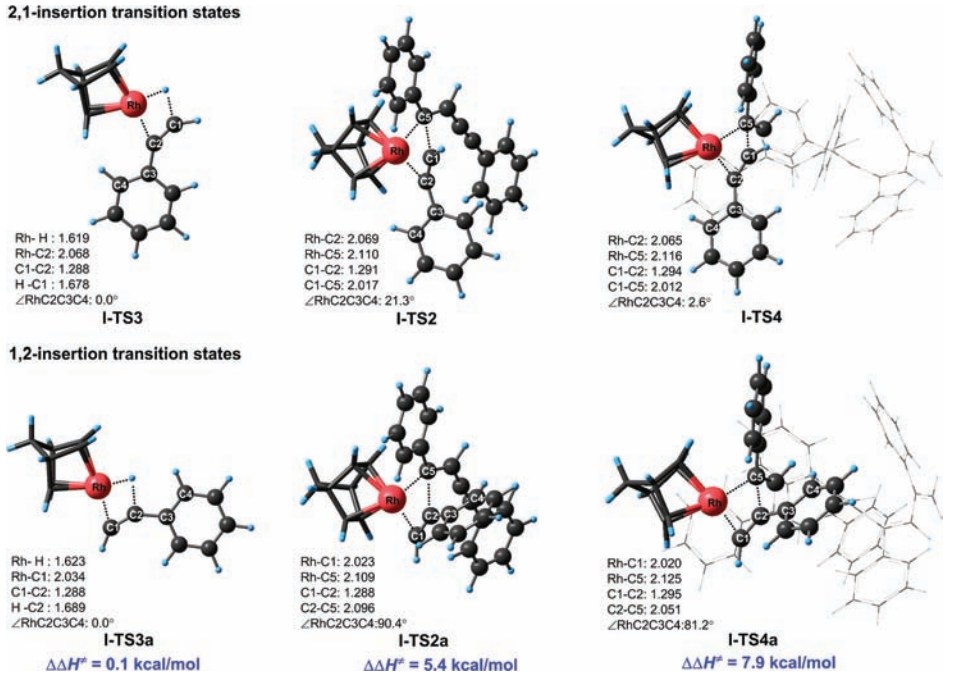

Figure 7. Optimized structures of 2,1-insertion/1,2-insertion transition states for different model systems (**I-TS2**/**2a** and **I-TS3**/**3a** are QM models, and **I-TS4**/**4a** are ONIOM models). Bond lengths are in angstroms. Enthalpies were corrected for solvation effect.

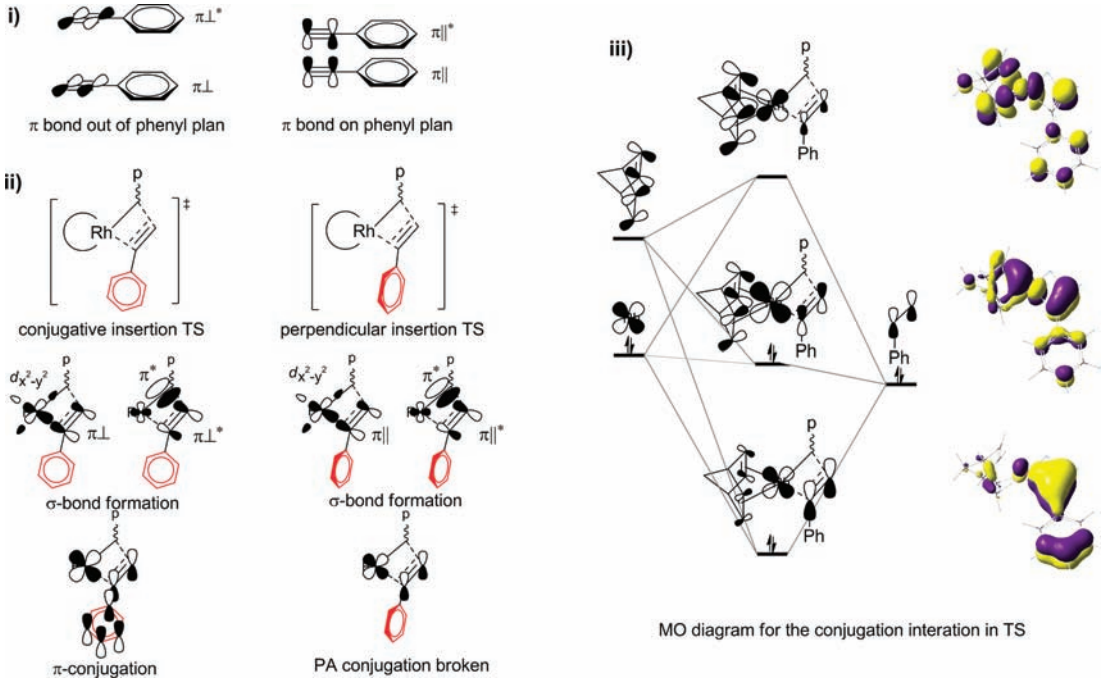

Figure 8. Electronic characteristics of the conjugative insertion transition state and its molecular orbital diagram: (i) π orbitals of the triple bond of PA, (ii) preferred (conjugative) and less favored (nonconjugative) perpendicular insertion transition state, and (iii) MO diagram to illustrate the conjugative character of the insertion transition state.

regioselectivity during the polymerization, we further carried out an ONIOM study for both 2,1- and 1,2-insertion utilizing a "real" model with six monomers in the propagation chain (see **I-TS4** and **I-TS4a** in Figure 7). We found that the preference of 2,1-insertion over 1,2-insertion increases up to 7.9 kcal/mol. The preference increases with increasing bulk of the propagation chain, as shown in Figure 7. The bulky propagating chains obviously interfere with the conjugative interaction of the insertion transition state for 1,2-insertion. In **I-TS2a** and **I-TS4a**, the $\angle \mathrm{RhCCC}^{\mathrm{phenyl}}$ angles are calculated to be 90.4° and 81.2°, respectively, which are much higher than the corresponding angles in **I-TS2** and **I-TS4** for 2,1-insertion. The high preference

dx.doi.org/10.1021/ja2012565 |*J. Am. Chem. Soc.* 2011, 133, 7926–7941

Scheme 5. Pathways to PPA with Different Stereoregularities

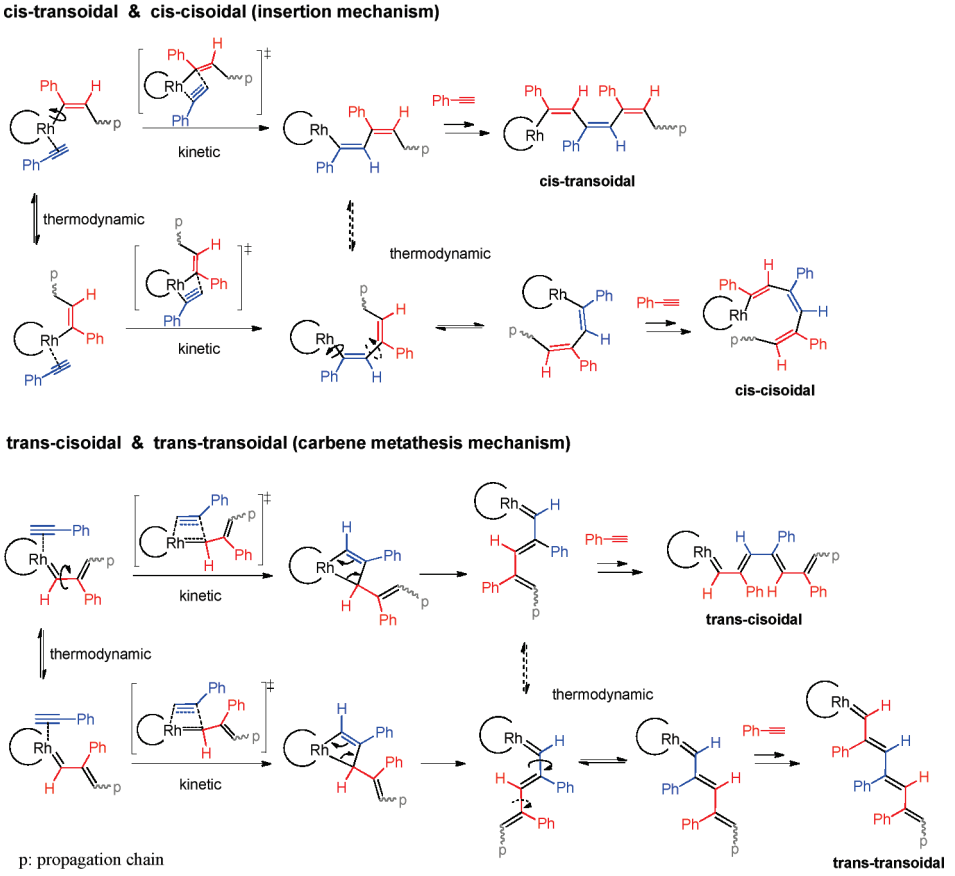

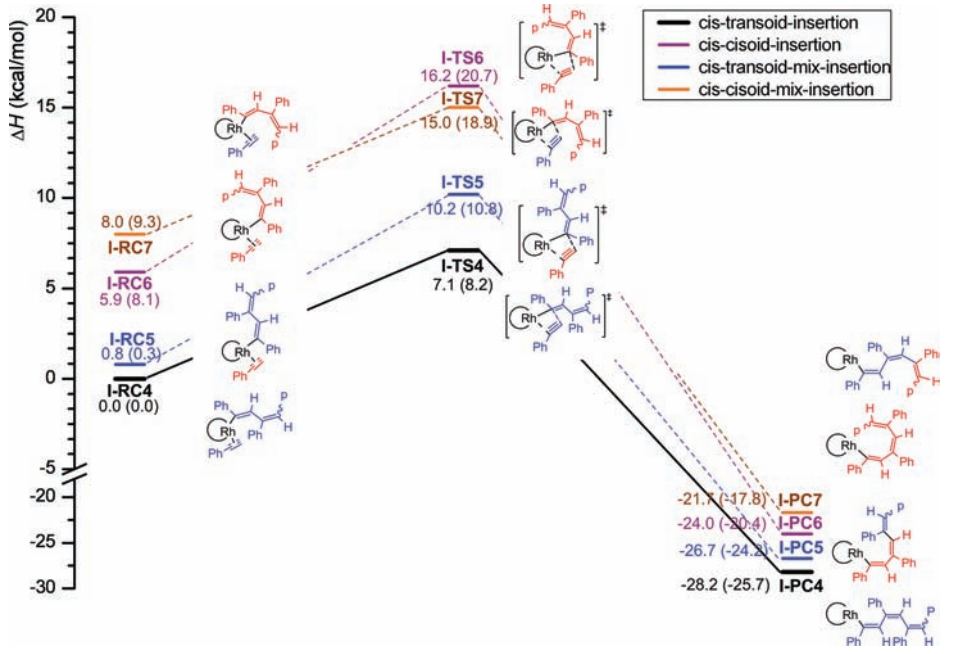

Figure 9. ONIOM PES profiles for the reaction pathways producing different stereoconformers of PPA. (*p* = polymer chain; nbd ligand is simplified as a curve for clarity). Solvent-corrected enthalpies and free energies (in parentheses) are in kcal/mol, relative to the ONIOM model **I-RC4**. The *cis*−*transoidal* and *cis*−*cisoidal* chains are highlighted in blue and red, respectively.

for 2,1-insertion revealed with the "real" model can well explain that only head-to-tail structures were found in experiments.[7,16]

Actually, due to the conjugative characteristic of PA insertion transition state, it can be expected that the Rh-catalyzed PA

dx.doi.org/10.1021/ja2012565 |*J. Am. Chem. Soc.* 2011, 133, 7926–7941

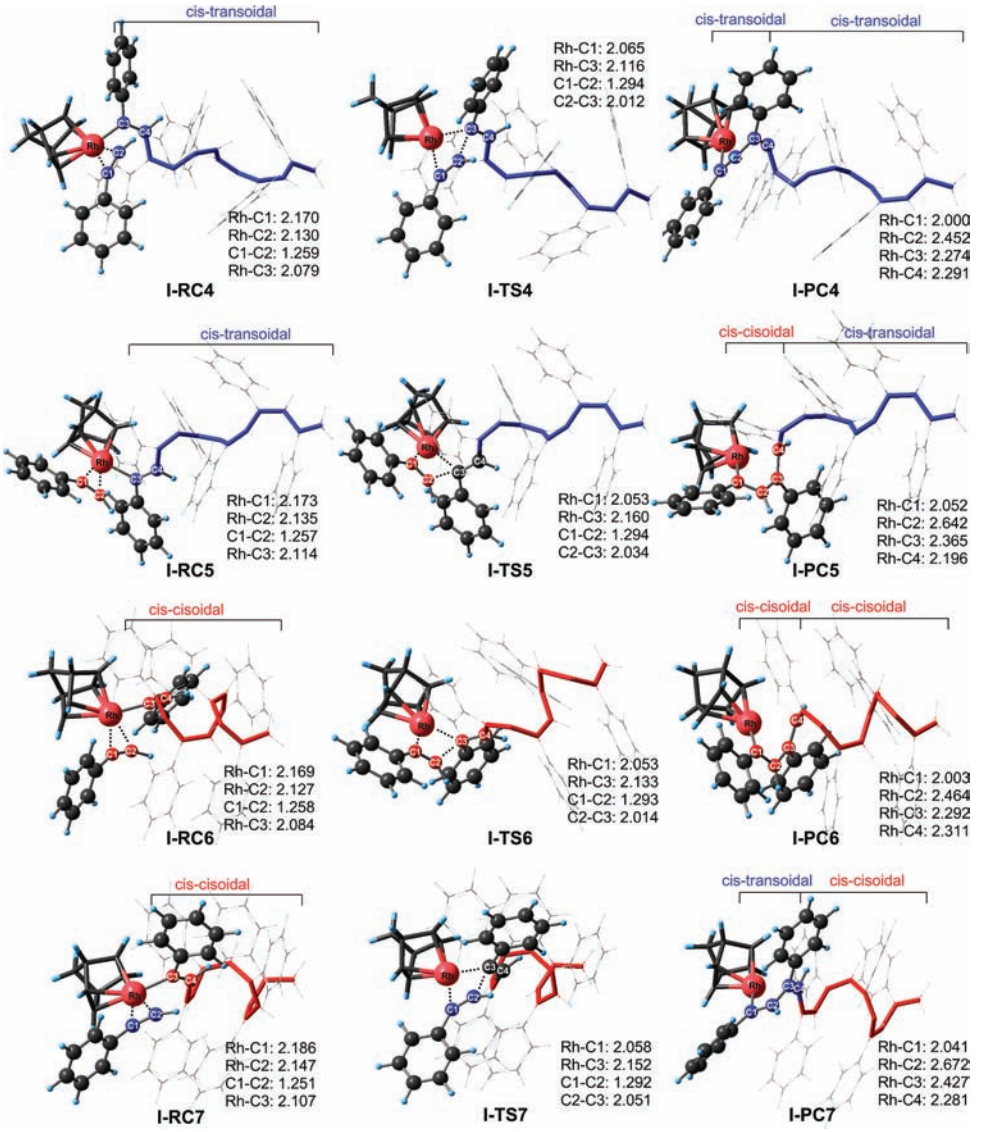

Figure 10. ONIOM optimized structures along the reaction pathways leading to different stereoconformers of PPA. Bond lengths are in angstroms. The *cis−transoidal* and *cis−cisoidal* units are highlighted in blue and red, respectively.

polymerization predominantly prefers 2,1-insertion,[16] which should be quite different from the polymerization of substituted alkenes.[106−108]

3.4. Stereoregularity. There exist theoretically four types of stereoregular structures for poly-PA: the *cis−transoidal*, *cis−cisoidal*, *trans−transoidal*, and *trans−cisoidal* structures, as shown in Figure 1(v). These types of stereoregular structures composed of alternative single and double bonds could be controlled by both kinetic and thermodynamic factors. The rotation around the single bond would lead to the interchange between *cis−transoid* and *cis−cisoid*, or between *trans−transoid* and *trans−cisoid*. This single bond rotation has a low barrier, is under thermodynamic control, and is supposed to be sensitive to the intramolecular interaction of PPA derivatives or to the environmental surroundings. The other important factor is the kinetic control, which is determined by the energy of the insertion transition state that leads to specific stereoregular structure. As shown in the top of Scheme 5, under regioregular 2,1-insertion, *cis−transoidal* and *cis−cisoidal* product structures can be obtained through two isomers of the insertion TS connected by the rotation of the Rh−polymer single bond. The *cis−transoidal* and *cis−cisoidal* units formed via different TSs again can interchange via single bond rotation based on their thermodynamic stabilities.

In contrast to the insertion mechanism, the carbene metathesis mechanism leads to the *trans−transoidal* or *trans−cisoidal* structures via different metathesis TS isomers, which are connected by the rotation of the single bond adjacent to Rh-carbene, as shown at the bottom of Scheme 5. After the ring-opening, single bond rotation also leads to thermodynamic interchange between *trans−transoidal* and *trans−cisoidal* structures. Herein, we discuss the stereoregularity on the basis of the Rh^I 2,1-insertion mechanism, because we determined in the preceding section that the Rh-catalyzed polymerization of PA preferentially proceeds via the Rh^I insertion mechanism with 2,1-insertion regioselectivity.

In order to reveal the factors that control the polymer stereoregularity via Rh^I insertion mechanism, four types of reaction

dx.doi.org/10.1021/ja2012565 |*J. Am. Chem. Soc.* 2011, 133, 7926–7941

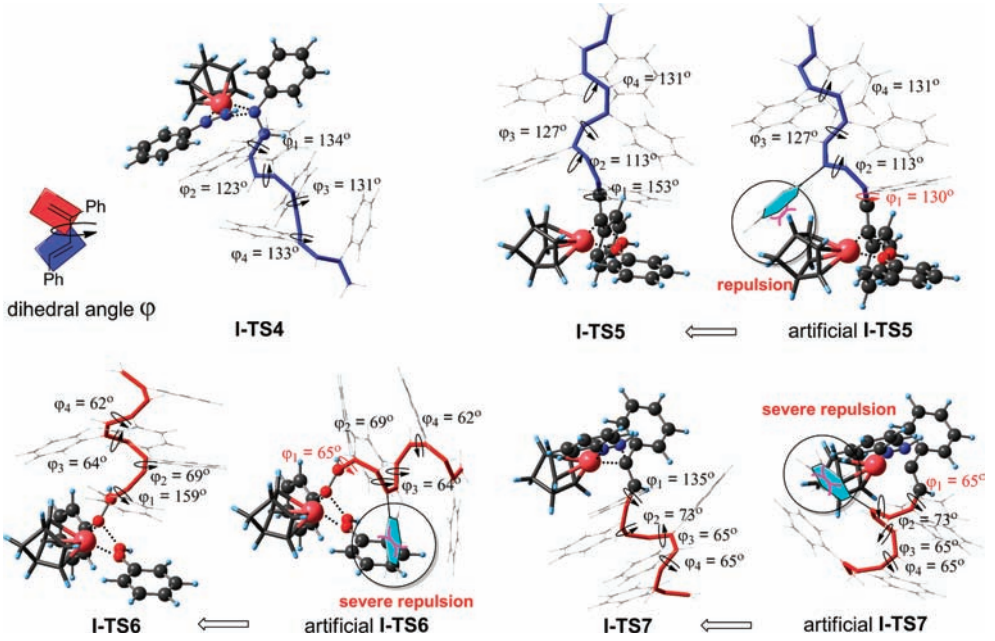

Figure 11. Steric repulsion in the transition states leading to different stereoconformers of PPA. φ is the dihedral angle between two monomer units. An artificial transition state is constructed by changing the constrained φ_1 dihedral angle in the true transition state back to the average dihedral angle value in the optimal *cis*−*transoidal* or *cis*−*cisoidal* conformer. The *cis*−*transoidal* and *cis*−*cisoidal* chains are highlighted in blue and red, respectively.

pathways for the *cis*−*transoidal* and *cis*−*cisoidal* polymer structures were studied with Rh^I-polymer models using the ONIOM method: (1) the *cis*−*transoid*-insertion **4** (**I-RC4** → **I-TS4** → **I-PC4**), where PA incorporates into a *cis*−*transoidal* parent chain leading to a pure *cis*−*transoidal* polymer chain; (2) the *cis*−*transoid*-mix-insertion **5** (**I-RC5** → **I-TS5** → **I-PC5**), where PA enters into a *cis*−*transoidal* parent chain resulting in a *cis*−*cisoidal* dyad in the *cis*−*transoidal* polymer; (3) the *cis*−*cisoid*-insertion **6** (**I-RC6** → **I-TS6** → **I-PC6**), where PA binds to a *cis*−*cisoidal* parent chain producing a pure *cis*−*cisoidal* polymer chain; and (4) the *cis*−*cisoid*-mix-insertion **7** (**I-RC7** → **I-TS7** → **I-PC7**), where PA inserts into a *cis*−*cisoidal* parent chain introducing a *cis*−*transoidal* dyad in the *cis*−*cisoidal* polymer chain. We selected a polymer model consisting of six repeated monomer units, as this length roughly represents one layer of helical *cis*−*transoidal* polymer structure. The last monomer in the chain, the inserting PA, and the catalyst were treated quantum mechanically, and the rest of the propagation chain was treated by UFF molecular mechanics. The PES profiles are shown in Figure 9. Optimized structures and key parameters are depicted in Figure 10.

We found that the models **4** and **5** with a *cis*−*transoidal* parent chain have much higher reactivity for the PA insertion as compared with the models **6** and **7** with a *cis*−*cisoidal* parent chain. The *cis*−*transoid*-insertion and *cis*−*transoid*-mix-insertion only need to surmount the reaction barriers of 7.1 and 10.2 kcal/mol, respectively. However, the PA insertions into a *cis*−*cisoidal* parent chain have to overcome reaction barriers higher than 15 kcal/mol, as shown in Figure 9. *Our results strongly suggest that the polymerization adopting a cis*−*transoidal conformation is much more kinetically favorable*. For models with a *cis*−*transoidal* parent chain, the *cis*−*transoid*-insertion pathway (**I-TS4**) is more favorable than the *cis*−*transoid*-mix-insertion (**I-TS5**) by 3.1 kcal/mol, while for models with a *cis*−*cisoidal* parent chain, the *cis*−*cisoidal*-mix-insertion is slightly preferred; the transition-state enthalpy of **I-TS7** is lower than for **I-TS6** by 1.2 kcal/mol. These results indicate that the PA insertion prefers to form a *cis*−*transoidal* dyad for either a *cis*−*transoidal* or a *cis*−*cisoidal* parent chain. Through the PES profiles in Figure 9, one can see that the relative energies of the transition states correlate well with those of the corresponding reactants and products. The kinetically favorable *cis*−*transoid*-insertion pathway produces the most thermodynamically stable product, **I-PC4**.

The kinetic differences for the stereoconformationally selective insertion mainly originate from the steric effect, since there are no typical electron-donating/-withdrawing groups in the studied model systems. The polymer chain adopts a screw-sense helical structure in these species. The calculated dihedral angle φ for each monomer dyad ranges from 120° to 140° for *cis*−*transoid*. The *cis*−*cisoidal* helix is calculated to have the dihedral angle φ between 60° and 70°. To illustrate the structural changes in the TS, the dihedral angles of each dyad in the helical chains are depicted in Figure 11. The transition state **I-TS4** has a normal helical *cis*−*transoidal* parent chain, where the dihedral angles φ_{1-4} are all close to 130°, indicating that the parent chain dose not encounter significant steric constraint during PA insertion. However, in **I-TS5**, φ_1 (153°) deviates significantly from its normal value. By artificially changing the parent chain back to a normal helical *cis*−*cisoidal* structure by altering φ_1 to the average value 130°, we find that the phenyl group of the third PA monomer in the parent chain locates very close to the nbd ligand (see artificial **I-TS5** in Figure 11). This steric repulsion results in the deviation of φ_1 in **I-TS5** to 153°. Evidence can also be seen that the bond lengths of $Rh-C^3$ and C^2-C^3 in **I-TS5** are longer than those in **I-TS4** due to the steric repulsion (Figure 10). The transition states **I-TS6** and **I-TS7** have more significant changes in the parent chain during PA insertion. The helical *cis*−*cisoidal* structure has thinner layers and thus has less space for PA insertion. In **I-TS6**, the dyad adjacent to rhodium has already changed to *cis*−*transoidal* conformation ($\varphi^1 = 159°$). From the artificial **I-TS6** ($\varphi^1 = 65°$), we find that the third phenyl

dx.doi.org/10.1021/ja2012565 |*J. Am. Chem. Soc.* 2011, 133, 7926–7941

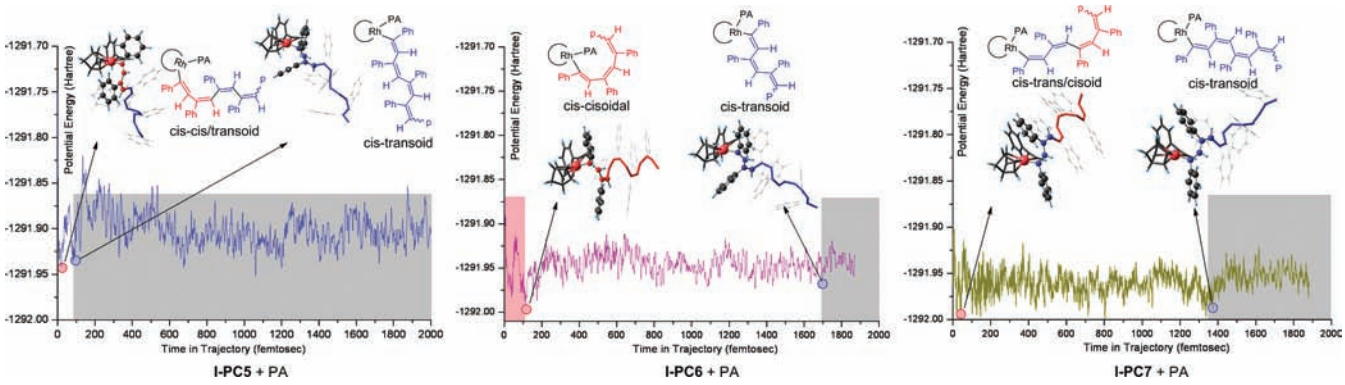

Figure 12. ONIOM ADMP simulations for the conformation changes of non-*cis*−*transoidal* model chain in **I-PC5/6/7** + PA. The *cis*−*transoidal* and *cis*−*cisoidal* units are highlighted in blue and red, respectively (*p* = polymer chain; nbd ligand is simplified as a curve for clarity). The structures shown are optimized minima from the snapshot of the trajectories. Background color: gray-blue, chain in *cis*−*transoidal* conformation; white, chain in mixed *cis*−*cisoidal/transoidal* conformation; pink, chain in *cis*−*cisoidal* conformation.

group of the chain already overlaps with the inserting PA monomer, indicating a severe steric repulsion. **I-TS7** has a similar situation to **I-TS6**. The artificial **I-TS7** depicted a severe steric repulsion between the third phenyl group and the nbd ligand. It is not surprising that PA insertion into the *cis*−*cisoidal* parent chain is highly unfavorable because of these severe repulsions. The *cis*−*transoidal* or *cis*−*cisoidal* chain can adopt either a right-handed helical conformation or a left-handed helical conformation. The studied Rh catalyst with nbd ligand has mirror symmetry; therefore, it shows no preference toward right-handed or left-handed helix (Figures S8−S12). It can be anticipated that an asymmetric ligand in the catalyst or chiral/bulky PA derivatives should be required, to achieve helical chirality for PPA.

For the dynamics of isomerization of the nascent polymer chains before the next insertion step, we have performed ADMP simulations in the gas phase using **I-PC5**+PA, **I-PC6**+PA, and **I-PC7**+PA as starting points and found that their isomerizations to *cis*−*transoidal* conformation are facile, as shown in Figure 12. The **I-PC5**+PA with a *cis*−*transoidal* chain mixed with a *cis*−*cisoidal* dyad changes into pure *cis*−*transoidal* structure quickly, in ∼80 fs. The **I-PC6**+PA bearing a pure *cis*−*cisoidal* model chain also changes into pure *cis*−*transoidal* conformer after ∼1700 fs. The **I-PC7**+PA possessing a *cis*−*cisoidal* chain mixed with a *cis*−*transoidal* dyad relaxes to pure *cis*−*transoidal* structure slightly faster, at 1400 fs. Experimental study also suggested the thermoreversible *cis*−*cisoidal* to *cis*−*transoidal* isomerization in polymerization chains.[109] Therefore, a parent chain with a *cis*−*transoidal* conformer is thermodynamically accessible via isomerization before the next insertion. The stereoregularity of the PPA is mainly controlled by the kinetic factor that highly prefers the *cis*−*transoid*-insertion into a *cis*−*transoidal* parent chain. This well explains that *cis*−*transoidal* PPA polymers are widely observed for Rh-catalyzed systems.[6,7] Because the kinetic factor specifically prefers a *cis*−*transoid* stereoconformer, in order to obtain other stereoconformation of PPA with Rh catalysts, we need to switch to controlling the thermodynamic factor by, for example, introducing intramolecular or intermolecular interactions with substituted PA or utilizing environmental stimuli.[9,110] However, we still cannot rule out the possibility of altering the kinetic properties of the insertion TS to change the stereoregularity, supposing that functional groups of the Rh catalyst could alter the conformation of the transition state via interacting with functionalized PA in the polymer chain.

4. CONCLUSIONS

We have presented detailed DFT, ONIOM, and ONIOM-MD studies to reveal the mechanisms of Rh-catalyzed polymerization of phenylacetylene and the factors controlling its regioselectivity and stereochemistry, with a classical nbd-rhodium catalyst system $[Rh(nbd)Cl]_2$. The Rh-catalyzed polymerization of PA proceeds via the Rh^I insertion mechanism, although all the Rh^I, Rh^{III}, and Rh-carbene types of intermediates are calculated to be thermodynamically and kinetically feasible at room temperature in solution. The Rh^I insertion mechanism is calculated to have a propagation activation enthalpy of ∼9 kcal/mol, much lower than those of the Rh-carbene metathesis mechanism ($\Delta H^{\ddagger} \approx 25$ kcal/mol for the rate-determining step) and the Rh^{III} insertion mechanism ($\Delta H^{\ddagger} \approx 22$ kcal/mol). Our study suggested that PA insertion into the Rh-phenylalkynyl bond is possible as the initial insertion step. There exists a quick pre-equilibrium between the phenylethynyl-Rh^I and hydride-diphenylethynyl-Rh^{III} intermediates during the initiation stage.

The Rh^I insertion mechanism prefers a 2,1-insertion, leading to head-to-tail regioselective PPA. The preference for 2,1-insertion over 1,2-insertion increases with increasing bulk of the propagated chain. The 2,1-insertion is favored over 1,2-insertion by up to 7.9 kcal/mol with the ONIOM model. Our study found a unique π-conjugative characteristic for the insertion transition state, in which a conjugative network is formed by the conjugative PA, the Rh d_π orbital, and the π acceptor nbd ligand, to gain extra stabilization energy. This conjugative characteristic of the insertion transition state always causes steric repulsion between the phenyl group of PA and the bulky propagation chain, probably exclusively preferring the 2,1-insertion. This provides a new understanding for tuning 2,1-/1,2-selectivity during polymerization of PA.

Kinetic factors play a key role in the stereoconformational selectivity. PA monomer highly prefers to insert into a parent propagation chain in a *cis*−*transoidal* conformer rather than a *cis*−*cisoidal* conformer ($\Delta\Delta H^{\ddagger} \geq 4.8$ kcal/mol). The propagation chain can easily adopt a *cis*−*transoidal* conformation via single bond rotation before the next insertion. The kinetic difference mainly originates from steric repulsion caused by the conformational constraint of the parent propagation chain during insertion. To tailor the stereoregularity of the PPA catalyzed by Rh catalysts, it is important to distinguish kinetic control from

dx.doi.org/10.1021/ja2012565 |*J. Am. Chem. Soc.* 2011, 133, 7926–7941

thermodynamic control. Asymmetric ligands in the catalyst or chiral/bulky PA derivatives are suspected to be necessary to achieve helical chirality.

■ ASSOCIATED CONTENT

Supporting Information. Complete refs 63 and 73; figures, schemes, and tables containing detailed information about other reaction pathways; figures showing the key structures; and Cartesian coordinates for all the stationary points. This material is available free of charge via the Internet at http://pubs.acs.org.

■ AUTHOR INFORMATION

Corresponding Author
morokuma@fukui.kyoto-u.ac.jp

■ ACKNOWLEDGMENT

We thank Dr. Lung Wa Chung and Dr. Fengyi Liu for helpful discussion. Z.K. acknowledges the Fukui Institute Fellowship. This work is in part supported by the Japan Science and Technology Agency (JST) with a Core Research for Evolutional Science and Technology (CREST) grant in the Area of High Performance Computing for Multiscale and Multiphysics Phenomena. Computer resources allocated at Research Center of Computer Science (RCCS) at the Institute for Molecular Science (IMS) are also acknowledged.

■ REFERENCES

(1) Chiang, C. K.; Fincher, C. R.; Park, Y. W.; Heeger, A. J.; Shirakawa, H.; Louis, E. J.; Gau, S. C.; Macdiarmid, A. G. *Phys. Rev. Lett.* **1977**, *39*, 1098–1101.
(2) Shirakawa, H.; Louis, E. J.; Macdiarmid, A. G.; Chiang, C. K.; Heeger, A. J. *J. Chem. Soc., Chem. Commun.* **1977**, 578–580.
(3) MacDiarmid, A. G. *Angew. Chem., Int. Ed.* **2001**, *40*, 2581–2590.
(4) Shirakawa, H. *Angew. Chem., Int. Ed.* **2001**, *40*, 2575–2580.
(5) Heeger, A. J. *Angew. Chem., Int. Ed.* **2001**, *40*, 2591–2611.
(6) Akagi, K. *Chem. Rev.* **2009**, *109*, 5354–5401.
(7) Liu, J. Z.; Lam, J. W. Y.; Tang, B. Z. *Chem. Rev.* **2009**, *109*, 5799–5867.
(8) Aoki, T.; Kaneko, T.; Teraguchi, M. *Polymer* **2006**, *47*, 4867–4892.
(9) Lam, J. W. Y.; Tang, B. Z. *Acc. Chem. Res.* **2005**, *38*, 745–754.
(10) Yashima, E.; Maeda, K. *Macromolecules* **2008**, *41*, 3–12.
(11) Kakuchi, R.; Shimada, R.; Tago, Y.; Sakai, R.; Satoh, T.; Kakuchi, T. *J. Polym. Sci., Part A: Polym. Chem.* **2010**, *48*, 1683–1689.
(12) Maeda, K.; Tamaki, S.; Tamura, K.; Yashima, E. *Chem. Asian J.* **2008**, *3*, 614–624.
(13) Maeda, K.; Yashima, E. *J. Synth. Org. Chem. Jpn.* **2002**, *60*, 878–890.
(14) Yashima, E. *Anal. Sci.* **2002**, *18*, 3–6.
(15) Yashima, E.; Maeda, K.; Iida, H.; Furusho, Y.; Nagai, K. *Chem. Rev.* **2009**, *109*, 6102–6211.
(16) Mayershofer, M. G.; Nuyken, O. *J. Polym. Sci., Part A: Polym. Chem.* **2005**, *43*, 5723–5747.
(17) Ejfler, J.; Kobylka, M.; Hojniak, M.; Sobota, P. *J. Mol. Catal. A-Chem.* **2004**, *224*, 93–96.
(18) Ohff, A.; Burlakov, V. V.; Rosenthal, M. *J. Mol. Catal. A* **1969**, *108*, 119.
(19) Masuda, T.; Hasegawa, K. I.; Higashim, T *Macromolecules* **1974**, *7*, 728–731.
(20) Masuda, T.; Sasaki, N.; Higashimura, T. *Macromolecules* **1975**, *8*, 717–721.
(21) Xu, K. T.; Peng, H.; Lam, J. W. Y.; Poon, T. W. H.; Dong, Y. P.; Xu, H. Y.; Sun, Q. H.; Cheuk, K. K. L.; Salhi, F.; Lee, P. P. S.; Tang, B. Z. *Macromolecules* **2000**, *33*, 6918–6924.
(22) Petit, A.; Moulay, S.; Aouak, T. *Eur. Polym. J.* **1999**, *35*, 953–963.
(23) Trepka, W. J.; Sonnenfe, R. J. *J. Polym. Sci. A1* **1970**, *8*, 2721.
(24) Ravikumar, L.; Thevi, R. *Polym. Sci. Ser. B+* **2008**, *50*, 227–231.
(25) Furlani, A.; Napoletano, C.; Russo, M. V.; Camus, A.; Marsich, N. *J. Polym. Sci., Part A: Polym. Chem.* **1989**, *27*, 75–86.
(26) Katayama, H.; Yamamura, K.; Miyaki, Y.; Ozawa, F. *Organometallics* **1997**, *16*, 4497–4500.
(27) Goldberg, Y.; Alper, H. *J. Chem. Soc., Chem. Commun.* **1994**, 1209–1210.
(28) Kishimoto, Y.; Itou, M.; Miyatake, T.; Ikariya, T.; Noyori, R. *Macromolecules* **1995**, *28*, 6662–6666.
(29) Schniedermeier, J.; Haupt, H. J. *J. Organomet. Chem.* **1996**, *506*, 41–47.
(30) Zhang, Y.; Wang, D. R.; Wurst, K.; Buchmeiser, M. R. *J. Organomet. Chem.* **2005**, *690*, 5728–5735.
(31) Kishimoto, Y.; Eckerle, P.; Miyatake, T.; Kainosho, M.; Ono, A.; Ikariya, T.; Noyori, R. *J. Am. Chem. Soc.* **1999**, *121*, 12035–12044.
(32) Misumi, Y.; Masuda, T. *Macromolecules* **1998**, *31*, 7572–7573.
(33) Misumi, Y.; Kanki, K.; Miyake, M.; Masuda, T. *Macromol. Chem. Phys.* **2000**, *201*, 2239–2244.
(34) Saeed, I.; Shiotsuki, M.; Masuda, T. *Macromolecules* **2006**, *39*, 8567–8573.
(35) Jimenez, M. V.; Perez-Torrente, J. J.; Bartolome, M. I.; Vispe, E.; Lahoz, F. J.; Oro, L. A. *Macromolecules* **2009**, *42*, 8146–8156.
(36) Li, K. L.; Wei, G. P.; Darkwa, J.; Pollack, S. K. *Macromolecules* **2002**, *35*, 4573–4576.
(37) Li, K.; Mohlala, M. S.; Segapelo, T. V.; Shumbula, P. M.; Guzei, I. A.; Darkwa, J. *Polyhedron* **2008**, *27*, 1017–1023.
(38) Furlani, A.; Licoccia, S.; Russo, M. V.; Camus, A.; Marsich, N. J. Polym. Sci., Part A: Polym. Chem. **1986**, *24*, 991–1005.
(39) Rodriguez, J. G.; Lafuente, A.; Arranz, J. *J. Polym. Sci., Part A: Polym. Chem.* **2005**, *43*, 6438–6444.
(40) Furlani, A.; Collamat., I; Sartori, G. *J. Organomet. Chem.* **1969**, *17*, 463–&.
(41) Tabata, M.; Yang, W.; Yokota, K. *Polym. J. (Tokyo, Jpn.)* **1990**, *22*, 1105–1107.
(42) Tabata, M.; Sone, T.; Sadahiro, Y. *Macromol. Chem. Phys.* **1999**, *200*, 265–282.
(43) Tang, B. Z.; Poon, W. H.; Leung, S. M.; Leung, W. H.; Peng, H. *Macromolecules* **1997**, *30*, 2209–2212.
(44) Trzeciak, A. M.; Ziolkowski, J. J. *Appl. Organomet. Chem.* **2004**, *18*, 124–129.
(45) Saeed, I.; Shiotsuki, M.; Masuda, T. *J. Mol. Catal. A-Chem.* **2006**, *254*, 124–130.
(46) Abe, S.; Hirata, K.; Ueno, T.; Morino, K.; Shimizu, N.; Yamamoto, M.; Takata, M.; Yashima, E.; Watanabe, Y. *J. Am. Chem. Soc.* **2009**, *131*, 6958–.
(47) Onishi, N.; Shiotsuki, M.; Sanda, F.; Masuda, T. *Macromolecules* **2009**, *42*, 4071–4076.
(48) Lynam, J. M. *Chem.—Eur. J.* **2010**, *16*, 8238–8247.
(49) Vastine, B. A.; Hall, M. B. *Organometallics* **2008**, *27*, 4325–4333.
(50) Cowley, M. J.; Lynam, J. M.; Slattery, J. M. *Dalton Trans.* **2008**, 4552–4554.
(51) Experiments showed that there are no cyclohexadiene and polyphenylene structure sequences in PPA, and radical inhibitors have no negative effects on the polymerization.[2529]
(52) Alonso-Moreno, C.; Carrillo-Hermosilla, F.; Romero-Fernandez, J.; Rodriguez, A. M.; Otero, A.; Antinolo, A. *Adv. Synth. Catal.* **2009**, *351*, 881–890.
(53) Beller, M.; Trauthwein, H.; Eichberger, M.; Breindl, C.; Muller, T. E. *Eur. J. Inorg. Chem.* **1999**, 1121–1132.
(54) Beller, M.; Trauthwein, H.; Eichberger, M.; Breindl, C.; Herwig, J.; Muller, T. E.; Thiel, O. R. *Chem.—Eur. J.* **1999**, *5*, 1306–1319.
(55) Haynes, A.; Haslam, C. E.; Bonnington, K. J.; Parish, L.; Adams, H.; Spey, S. E.; Marder, T. B.; Coventry, D. N. *Organometallics* **2004**, *23*, 5907–5909.

(56) Wolf, J.; Werner, H.; Serhadli, O.; Ziegler, M. L. *Angew. Chem. Int. Ed. Engl.* **1983**, *22*, 414–416.
(57) Werner, H.; Wolf, J.; Alonso, F. J. G.; Ziegler, M. L.; Serhadli, O. *J. Organomet. Chem.* **1987**, *336*, 397–411.
(58) Werner, H.; Bachmann, P.; Laubender, M.; Gevert, O. *Eur. J. Inorg. Chem.* **1998**, 1217–1224.
(59) Gil-Rubio, J.; Laubender, M.; Werner, H. *Organometallics* **1998**, *17*, 1202–1207.
(60) Fujita, Y.; Misumi, Y.; Tabata, M.; Masuda, T. *J. Polym. Sci., Part A: Polym. Chem.* **1998**, *36*, 3157–3163.
(61) Ito, T.; Shirakawa, H.; Ikeda, S. *J. Polym. Sci., Part A: Polym. Chem.* **1975**, *13*, 1943–1950.
(62) Percec, V.; Rudick, J. G.; Peterca, M.; Aqad, E.; Imam, M. R.; Heiney, P. A. *J. Polym. Sci., Part A: Polym. Chem.* **2007**, *45*, 4974–4987.
(63) Percec, V.; *Chem.—Eur. J.* **2006**, *12*, 5731–5746.
(64) Nishimura, T.; Ichikawa, Y.; Hayashi, T.; Onishi, N.; Shiotsuki, M.; Masuda, T. *Organometallics* **2009**, *28*, 4890–4893.
(65) Yashima, E.; Huang, S. L.; Matsushima, T.; Okamoto, Y. *Macromolecules* **1995**, *28*, 4184–4193.
(66) Parr, R. G.; Yang, W. *Density-functional Theory of Atoms and Molecules*; Oxford Univ. Press: Oxford, 1989.
(67) Cramer, C. J.; Truhlar, D. G. *Phys. Chem. Chem. Phys.* **2009**, *11*, 10757–10816.
(68) Vreven, T.; Morokuma, K.; Farkas, O.; Schlegel, H. B.; Frisch, M. J. *J. Comput. Chem.* **2003**, *24*, 760–769.
(69) Svensson, M.; Humbel, S.; Froese, R. D. J.; Matsubara, T.; Sieber, S.; Morokuma, K. *J. Phys. Chem.* **1996**, *100*, 19357–19363.
(70) Schlegel, H. B.; Millam, J. M.; Iyengar, S. S.; Voth, G. A.; Daniels, A. D.; Scuseria, G. E.; Frisch, M. J. *J. Chem. Phys.* **2001**, *114*, 9758–9763.
(71) Schlegel, H. B.; Iyengar, S. S.; Li, X. S.; Millam, J. M.; Voth, G. A.; Scuseria, G. E.; Frisch, M. J. *J. Chem. Phys.* **2002**, *117*, 8694–8704.
(72) Iyengar, S. S.; Schlegel, H. B.; Millam, J. M.; Voth, G. A.; Scuseria, G. E.; Frisch, M. J. *J. Chem. Phys.* **2001**, *115*, 10291–10302.
(73) Frisch, M. J.; *Gaussian 09*, Revision A.02; Gaussian, Inc.: Wallingford, CT, 2009.
(74) Becke, A. D. *J. Chem. Phys.* **1993**, *98*, 5648–5652.
(75) Lee, C. T.; Yang, W. T.; Parr, R. G. *Phys. Rev. B* **1988**, *37*, 785–789.
(76) Vosko, S. H.; Wilk, L.; Nusair, M. *Can. J. Phys.* **1980**, *58*, 1200–1211.
(77) Fukui, K. *Acc. Chem. Res.* **1981**, *14*, 363.
(78) Fukui, K. *J. Phys. Chem.* **1970**, *74*, 4161–4163.
(79) Ehlers, A. W.; Bohme, M.; Dapprich, S.; Gobbi, A.; Hollwarth, A.; Jonas, V.; Kohler, K. F.; Stegmann, R.; Veldkamp, A.; Frenking, G. *Chem. Phys. Lett.* **1993**, *208*, 111–114.
(80) Couty, M.; Hall, M. B. *J. Comput. Chem.* **1996**, *17*, 1359–1370.
(81) Marenich, A. V.; Cramer, C. J.; Truhlar, D. G. *J. Phys. Chem. B* **2009**, *113*, 6378–6396.
(82) Rappe, A. K.; Casewit, C. J.; Colwell, K. S.; Goddard, W. A.; Skiff, W. M. *J. Am. Chem. Soc.* **1992**, *114*, 10024–10035.
(83) Grotjahn, D. B. *Chem.—Eur. J.* **2005**, *11*, 7146–7153.
(84) Aoki, T.; Kaneko, T.; Maruyama, N.; Sumi, A.; Takahashi, M.; Sato, T.; Teraguchi, M. *J. Am. Chem. Soc.* **2003**, *125*, 6346–6347.
(85) Nishimura, T.; Guo, X. X.; Ohnishi, K.; Hayashi, T. *Adv. Synth. Catal.* **2007**, *349*, 2669–2672.
(86) Hirao, K.; Ishii, Y.; Terao, T.; Kishimoto, Y.; Miyatake, T.; Ikariya, T.; Noyori, R. *Macromolecules* **1998**, *31*, 3405–3408.
(87) Nakazato, A.; Saeed, I.; Katsumata, T.; Shiotsuki, M.; Masuda, T.; Zednik, J.; Vohlidal, J. *J. Polym. Sci., Part A: Polym. Chem.* **2005**, *43*, 4530–4536.
(88) Schäfer, M.; Mahr, N.; Wolf, J.; Werner, H. *Angew. Chem. Int. Ed. Engl.* **1993**, *32*, 1315–1317.
(89) Rappert, T.; Nurnberg, O.; Mahr, N.; Wolf, J.; Werner, H. *Organometallics* **1992**, *11*, 4156–4164.
(90) Circu, V.; Fernandes, M. A.; Carlton, L. *Inorg. Chem.* **2002**, *41*, 3859–3865.
(91) Chow, P.; Zargarian, D.; Taylor, N. J.; Marder, T. B. *J. Chem. Soc., Chem. Commun.* **1989**, 1545–1547.
(92) Windmuller, B.; Wolf, J.; Werner, H. *J. Organomet. Chem.* **1995**, *502*, 147–161.
(93) Ward, R. M.; Batsanov, A. S.; Howard, J. A. K.; Marder, T. B. *Inorg. Chim. Acta* **2006**, *359*, 3671–3676.
(94) Rappert, T.; Nurnberg, O.; Werner, H. *Organometallics* **1993**, *12*, 1359–1364.
(95) Wakatsuki, Y.; Koga, N.; Werner, H.; Morokuma, K. *J. Am. Chem. Soc.* **1997**, *119*, 360–366.
(96) Suresh, C. H.; Koga, N. *J. Theor. Comput. Chem.* **2005**, *4*, 59–73.
(97) De Angelis, F.; Sgamellotti, A.; Re, N. *Organometallics* **2007**, *26*, 5285–5288.
(98) Grotjahn, D. B.; Zeng, X.; Cooksy, A. L. *J. Am. Chem. Soc.* **2006**, *128*, 2798–2799.
(99) Grotjahn, D. B.; Zeng, X.; Cooksy, A. L.; Kassel, W. S.; DiPasquale, A. G.; Zakharov, L. N.; Rheingold, A. L. *Organometallics* **2007**, *26*, 3385–3402.
(100) Grotjahn, D. B.; Zeng, X.; Cooksy, A. L.; Kassel, W. S.; DiPasquale, A. G.; Zakharov, L. N.; Rheingold, A. L. *Organometallics* **2008**, *27*, 3626–3626.
(101) Bianchini, C.; Mealli, C.; Meli, A.; Sabat, M. *Organometallics* **1985**, *4*, 421–422.
(102) Bianchini, C.; Mealli, C.; Meli, A.; Sabat, M.; Silvestre, J.; Hoffmann, R. *Organometallics* **1986**, *5*, 1733–1741.
(103) Werner, H.; Heinemann, A.; Windmuller, B.; Steinert, P. *Chem. Ber.* **1996**, *129*, 903–910.
(104) Bianchini, C.; Meli, A.; Peruzzini, M.; Vizza, F. *Organometallics* **1990**, *9*, 1146–1155.
(105) Angoy, M.; Bartolome, M. I.; Vispe, E.; Lebeda, P.; Jimenez, M. V.; Perez-Torrente, J. J.; Collins, S.; Podzimek, S. *Macromolecules* **2010**, *43*, 6278–6283.
(106) Izzo, L.; Napoli, M.; Oliva, L. *Macromolecules* **2003**, *36*, 9340–9345.
(107) Correa, A.; Galdi, N.; Izzo, L.; Cavallo, L.; Oliva, L. *Organometallics* **2008**, *27*, 1028–1029.
(108) Schellenberg, J. *Prog. Polym. Sci.* **2009**, *34*, 688–718.
(109) Percec, V.; Rudick, J. G.; Peterca, M.; Wagner, M.; Obata, M.; Mitchell, C. M.; Cho, W. D.; Balagurusamy, V. S. K.; Heiney, P. A. *J. Am. Chem. Soc.* **2005**, *127*, 15257–15264.
(110) Percec, V.; Rudick, J. G.; Peterca, M.; Heiney, P. A. *J. Am. Chem. Soc.* **2008**, *130*, 7503–7508.